Structures 38 (2022) 1326–1348

Contents lists available at ScienceDirect

Structures

journal homepage: www.elsevier.com/locate/structures

Flexural behaviour of circular reinforced concrete columns strengthened by glass fibre reinforced polymer wrapping system

Omar F. Otoom [a,*], Weena Lokuge [a], Warna Karunasena [a], Allan C. Manalo [a], Togay Ozbakkaloglu [b], Mohammad R. Ehsani [c]

[a] Centre for Future Materials (CFM), School of Engineering, University of Southern Queensland, Springfield, QLD 4300, Australia
[b] Ingram School of Engineering, Texas State University, United States
[c] University of Arizona and President of QuakeWrap, Inc., United States

ARTICLE INFO

Keywords:
GFRP wrapping system
Concrete columns
Flexural behaviour
Finite element modelling
Theoretical analysis

ABSTRACT

The use of prefabricated glass fibre reinforced polymer (GFRP) wrapping systems in retrofitting reinforced concrete (RC) columns has emerged to enhance the overall axial performance. However, the effect of these systems on columns subjected to bending is still limited although the flexural loading on columns in real life is inevitable. This paper presents experimental, numerical, and theoretical investigations on the flexural behaviour of circular RC columns strengthened by a GFRP wrapping system. A total of eight columns were prepared and tested under three point bending to determine the contribution of the GFRP wrapping system to the overall flexural performance. The annulus between the RC columns and the GFRP wraps was filled with epoxy or cementitious grout to ensure transfer and distribution of stresses. The load-midspan deflection responses and failure modes were presented and evaluated. Furthermore, a nonlinear finite element modelling (FEM) was conducted using ABAQUS software to simulate the performance of unwrapped and GFRP-wrapped columns under flexural loading. A theoretical analysis was also developed using the basic beam theory to obtain the flexural capacity of the tested columns and compare it with experimental and FEM results. A parametric analysis was carried out to assess the effect of varying the thickness of GFRP and infill, as well as the loading mode, on the flexural behaviour of RC columns. The results of experimental tests demonstrated that GFRP-wrapped columns with epoxy infills significantly enhanced the flexural load capacity whereas columns with grout infills showed a prominent enhancement in ductility and energy absorption. The results of FEM and theoretical analyses were in good agreement with experimental results. The results of the developed theoretical model were found to have a good correlation with the results of the parametric investigation. Overall, the GFRP wrapping system implemented in this study is an effective repair technique for structural RC columns subjected to flexural loading. The proposed theoretical model can be used by the practising engineers to design a composite repair system for deteriorated reinforced concrete columns.

1. Introduction

In recent decades, Fibre Reinforced Polymer (FRP) composites have been used predominantly as efficient construction materials for repair and strengthening of concrete and steel structures. These materials have overcome the disadvantages of the traditional retrofitting techniques such as concrete and steel jacketing [1–3]. This is due to the superior properties of FRP composites such as light weight, high strength, corrosion resistance, large creep strain, high fatigue resistance, less weight comparing to steel repairs and ease in installation [4–6]. Prefabricated FRP wrapping systems has been found an attractive and easy retrofitting technique [7] that can significantly enhance the strength and ductility of concrete columns [8–10]. The application of the prefabricated systems requires providing an infill material in the annular space between the deteriorated column and the FRP jacket. Mohammed et al. [11] reported that changing the properties of infill material can significantly affect the behaviour of the FRP composite system and limit its capacity to transfer stresses around the FRP jackets. Majority of the

* Corresponding author.
E-mail addresses: omar.otoom@usq.edu.au (O.F. Otoom), weena.lokuge@usq.edu.au (W. Lokuge), karu.karunasena@usq.edu.au (W. Karunasena), allan.manalo@usq.edu.au (A.C. Manalo), togay.oz@txstate.edu (T. Ozbakkaloglu), mo@quakewrap.com (M.R. Ehsani).

https://doi.org/10.1016/j.istruc.2022.02.071
Received 10 November 2021; Received in revised form 20 January 2022; Accepted 25 February 2022

studies proved the efficiency of these systems in restoring axial strength of repaired structural columns [11–20]. Nevertheless, structural columns are prone to sustain significant lateral loadings such as earth pressures, wind loads, wave actions, and earthquake loads. Li et al. [21] reported that damage in real columns initiated due to both compression and bending loadings. In some cases, lateral loads can exceed 30% of the vertical load such as in coastal and offshore structures [22], thus can impose bending moments and shear forces on the structural piles [23]. Consequently, this can initiate structural deficiencies which can lead to major drawbacks in the overall flexural performance of columns. For this reason, retrofitting of deficient columns in bending becomes imperative to maintain their performance under the effect of severe environmental conditions. Moreover, flexural cracks are one of the most visible failure types of bridge columns in real-world impact events [24] as shown in Fig. 1, as well as earthquake excitation [25]. Vehicle collisions can cause permanent bending deformations in the direction of the applied loads [26]. This emphasises the importance of flexural strengthening for structural columns to improve their performance in the occurrence of comparable events. Furthermore, in bridge design, columns with circular sections are more prevalent than any other sectional shapes. This is due to the ease of construction and utilising various confinement techniques, effectiveness in sustaining biaxial moments, and suitability for seismic prone areas that demand strength and ductility in all directions [27]. Nonetheless, understanding the effect of bending on rehabilitated structural columns is critical in the design process of all shapes since it is necessary for creating interaction diagrams, which have been used in several studies to assess the performance of various columns [28–31]. This is owing to their adequacy in determining column strength, which varies based on axial loads and moments. Since existing concrete columns are subjected to a wide range of loadings that can create flexural inadequacies, the influence of bending is becoming a more relevant topic to address but researchers have paid little attention to such behaviour.

Up to date, limited research has been conducted to investigate the effect of prefabricated FRP wrapping systems on the performance of RC columns subjected to flexural loading. Hadi et al. [12] investigated the behaviour of circular RC columns under different loading schemes including four point bending and reported that the columns wrapped with reactive powder concrete and carbon FRP jackets achieved the highest capacity. However, only one type of filling materials was considered in this study to fill the annular gap between the column and the surrounding jackets. Also, Hadi et al. [16] studied the behaviour of circular concrete columns under four-point bending. The study included testing of columns which were cast using GFRP jackets and concluded that this wrapping is more adequate when combined with longitudinal GFRP reinforcement. Nonetheless, neither annular gap nor infill materials were utilized in this study. Furthermore, the contribution of prefabricated GFRP systems on square concrete beams with simulated damage was investigated by Mohammed et al. [33]. The damaged sections were repaired by GFRP composite and a joint system filled with a shrinkage-compensating cementitious grout. The beams were tested under four point bending and the results showed that the GFRP jacket is effective in repairing flexural members with a damage located at the compression side rather than at the tension side.

Fig. 1. Real-world bending deformation due to an impact event [32]

The use of one thin laminate of the prefabricated bidirectional wraps PileMedic^{TM} (Patent No. US9376782B1 [34]) can replace two or more layers of fabrics that would be applied using the wet lay-up technique. The advantages of columns repair system using such thin laminates were identified by their efficiency in delivering circumferential confinement and suitability to provide a seamless shell around retrofitted columns [35]. In addition, the unidirectional prefabricated glass wraps can have a significant contribution to the flexural behaviour of earthquake-damaged RC columns under the effect of cyclic loading, as it was indicated that the flexural strength and ductility capacity of the damaged concrete columns were enhanced effectively over the original columns [36]. Moreover, they are preferred over other prefabricated wrapping techniques as their tensile strength is 3 to 10 times higher than other jacketing systems [37]. In real practices, the annular space between the PileMedic^{TM} shell and the retrofitted column can be filled with epoxy or grout materials to complete the repair system and to utilize a full composite behaviour. This type of prefabricated wrapping systems was used by several researchers to explore their contribution to the axial behaviour of different structural columns; however, no studies have investigated their performance in case of columns subjected to bending. Kaya et al. [14] investigated the performance of buckled steel columns subjected to axial compression whereas expansive concrete was used to fill the annular gap. Their test results revealed the efficiency of using this type of wrapping systems in improving the axial behaviour of steel columns. Also, Lokuge et al. [17] proved that GFRP-wrapped systems filled by grout and epoxy infills can have outstanding contribution to the axial behaviour of damaged timber columns. Additionally, Menkulasi et al. [19] tested damaged timber piles repaired by PileMedic^{TM} laminates with the annular gap filled with underwater grout or epoxy infills. The piles were tested under the effect of both axial and eccentric loading and the results revealed that the capacity of the repaired columns could be enhanced significantly over the undamaged columns. Karagah [20] characterized the behaviour, axial capacity and failure modes of corroded steel piles using FRP confined grout systems. The study concluded that the use of such systems can effectively restore the axial capacity of the uncorroded piles. Otoom et al. [38] investigated three different infill materials for PileMedic^{TM} wrap and found that the contribution of this wrapping system is significant for low strength infills in terms of strength, modulus of elasticity and failure modes. To date, very limited research is available in fully understanding the performance of such wrapping systems as well as the influence of varying the properties of infill materials on the overall structural behaviour. In addition, to the best of authors' knowledge, no studies have pointed out the contribution of this wrapping system to the flexural performance of circular concrete columns. Hence, further investigations are becoming crucial to manifest their benefits and effectiveness on the flexural behaviour of RC columns.

On top of experimental works, the use of finite element modelling and theoretical analysis have been widely used to investigate the behaviour and bonding mechanisms of FRP wrapped concrete. Berthet et al. [39] developed an analytical model to predict the ultimate behaviour of all FRP confined concretes. Analytical investigations were also performed by [28,40] to estimate the load and moment capacity of concrete filled FRP circular tubes and found to give reasonable results with those from the experiments. Reddy et al. [5] conducted FEM analysis using ANSYS software to explore the effect of unconfined concrete strength, steel ratio and thickness of FRP on the strength of RC piles subjected to compression and lateral loadings. Otoom et al. [38] recently

conducted a finite element analysis using ABAQUS software to simulate the compression behaviour of various GFRP-wrapped infill materials and the predicted results revealed a good correlation with experimental results and failure modes. The concrete damaged plasticity model was adapted in the aforementioned study to demonstrate the plastic behaviour of infills and the results provided an excellent agreement with experiments. Li et al. [21] conducted a parametric study using ANSYS software and studied the effect of the thickness, stiffness and fibre orientation of the FRP layers on the strength and stiffness of the repaired RC columns. Other studies considered the effect of the shape modifications on various column cross sections using FRP bonded jackets and post-tensioned FRP shells with expansive cement concrete [41]. Likewise, Mohammed et al. [42] carried out numerical investigations using ABAQUS software to investigate the influence of grout properties on the effectiveness of the prefabricated glass FRP repair system under compression. Their study revealed that the compressive strength and elastic modulus of grout can significantly influence the stress transfer between the core material and the surrounding jacket. Although most studies focused on confinement effectiveness of the FRP composite materials on the behaviour of concrete columns subjected to axial compression [20,21,39,43–49], only a few studies [50,51] have been considered with modelling the contribution of GFRP composites to the overall flexural behaviour of columns.

The limitations in research attempts that scrutinize the contribution of various infill materials used in the GFRP wrapping systems and their effect on the performance of structural columns under flexure, motivated this paper to investigate the flexural behaviour of RC columns retrofitted by GFRP wrapping system with infill materials having different properties. The columns were encapsulated by GFRP jackets made using the thin PileMedic^{TM} laminates and filled with grout or epoxy infill. The investigation of this study included finite element analysis using ABAQUS to predict the flexural load- midspan deflection behaviour as well as the variation in failure mechanisms. Moreover, the finite element models were validated and compared with experiments. In addition, a theoretical analysis was established to obtain the flexural capacities of the tested columns. This study provides remarkable insights and useful information about the flexural performance of GFRP-wrapped columns and can effectively contribute to the knowledge of designers and engineers on sufficient use of similar wrapping systems.

2. Experimental program

2.1. Test specimens

A total of eight full scale circular RC column specimens were tested under three-point bending. The bending investigations are commonly conducted using either three-point or four-point bending tests. In three-point flexural bending, the maximum stress is found beneath the loading point, while in four-point flexural bending, the maximum stress is constant along the section between loading points, which could prevent early failure. By focusing on the bending influence in the centre location and considering the limitations of the experimental study, the three-point bending test was used to better investigate the bending behaviour given that the optimum bending performance occurs. The testing program in the current study investigates the type of infill materials and its influence on the flexural performance of the RC columns. Tested columns were labelled according to their wrapping status and the type of infill material. The first letters U and C refer to unwrapped and GFRP-wrapped, respectively. The second letter (C) refers to the material type of the base columns which is concrete in this testing program. Finally, the third part if exists, refers to the type of the infill material used to fill the annulus between the base column and the GFRP jacket, where CM and E refer to the cementitious grout and epoxy infills, respectively. For instance, the column CC-CM stands for a GFRP-wrapped concrete column with annulus filled with cementitious grout. The experimental columns were divided into four groups based on the strengthening scheme and each testing was duplicated. Columns UC are the base columns without any strengthening. Columns CC were wrapped by two layers of GFRP laminates. Columns CC-CM and CC-E had a 30 mm thick annulus filled with grout and epoxy infills, respectively. The details of columns are shown in Table 1 according to their GFRP wrapping scheme.

The plan and sectional views of the control and strengthened columns are shown in Fig. 2. All base columns had a diameter of 250 mm with a length of 1270 mm and were reinforced with 6 N12 (1.4% reinforcement ratio) in the longitudinal direction and R8 in the transverse direction at a centre to centre spacing of 100 mm with a clear concrete cover of 30 mm. All reinforcement arrangements were provided to accomplish the requirements of AS3600-2009 Standards [52].

Fig. 3 shows the preparation of full-scale columns whereas the formwork of the specimens was made of plastic tubes with an inner diameter of 250 mm and a height of 1270 mm. The reinforcement cages were ordered from a local steel supplier with outer diameter of 190 mm to maintain a clear cover of 30 mm from all perimeters. The cages were placed inside the formwork and the tubes were properly supported at bottom ends before the concrete was poured and compacted using electric vibrators. After curing, two specimens were left without any strengthening as control columns (columns UC) and two other specimens were wrapped with two layers of the GFRP laminates plus an overlap of 200 mm without any infills as GFRP-wrapped columns (columns CC). Meanwhile, four GFRP jackets were prepared as discussed in the following section (Section 2.2) to accommodate the dimensions of GFRP-wrapped columns with infills. The jackets were left to cure for at least seven days before being utilised as a formwork throughout the installation of the infill materials. The annular space between the core RC columns and the surrounding wrap of columns CC-CM and CC-E was then filled with grout and epoxy, respectively. These infills were prepared and mixed in the proper quantities according to the instructions provided by manufacturers. Since loose debris and dust could adversely affect the bond between the concrete surface and the surrounding wrapping system, the concrete surface was first scrubbed with a brush to remove any visible loose particles, and then a generous amount of acetone was slathered over the surface before wiping it away with a rag, ensuring that all contaminants were removed prior to pouring of infills or application of GFRP wrap.

Table 1
Details of tested columns.

Column	Diameter (mm)		Infill Type	Infill Thickness (mm)	Strengthening with GFRP wrap
	Unwrapped	Wrapped			
UC1	250	–	–	–	–
UC2	250	–	–	–	–
CC1	250	250	–	–	GFRP jackets
CC2	250	250	–	–	GFRP jackets
CC-CM1	250	310	Grout (CM)	30	GFRP jackets
CC-CM2	250	310	Grout (CM)	30	GFRP jackets
CC-E1	250	310	Epoxy (E)	30	GFRP jackets
CC-E2	250	310	Epoxy (E)	30	GFRP jackets

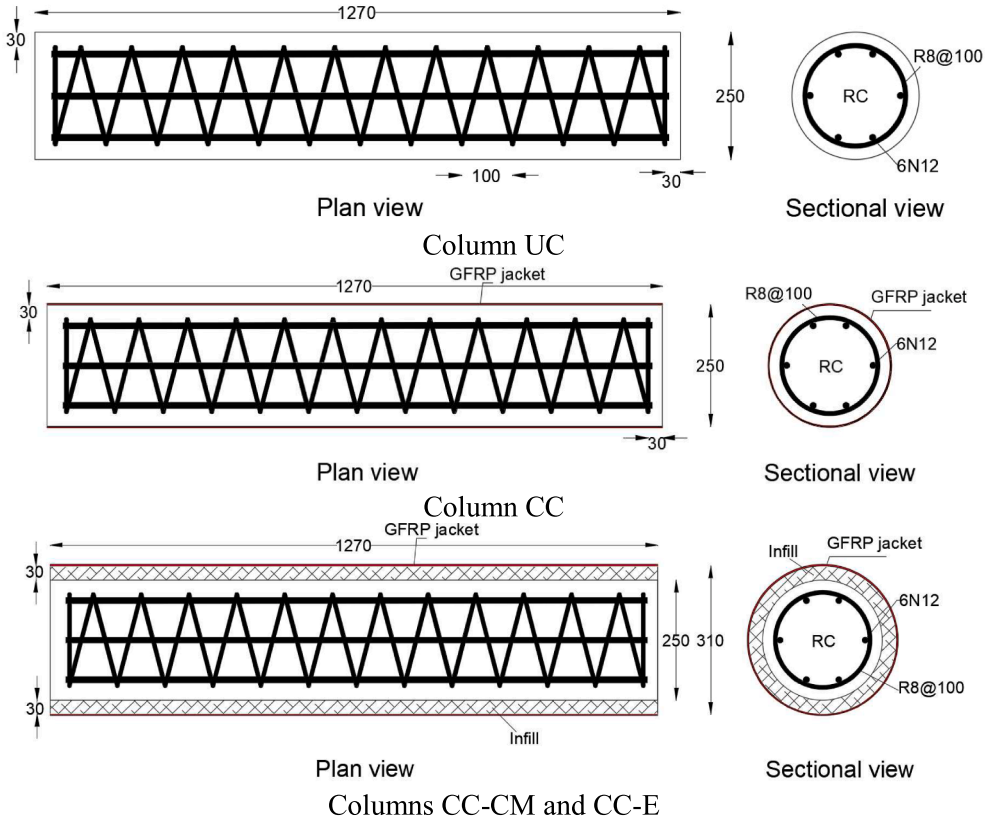

Fig. 2. Plan and sectional views of tested columns (all dimensions in mm).

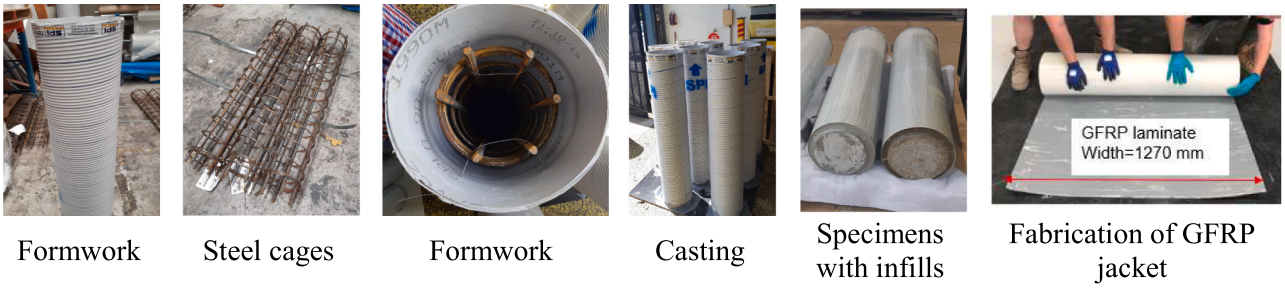

Fig. 3. Preparation of full-scale columns.

Table 2
Properties of GFRP (PLG60.60) laminate and resin according to manufacturers.

Material	Property	Value
PLG60.60 [53]	Tensile strength in longitudinal direction (MPa)	431
	Tensile strength in transverse direction (MPa)	418
	Modulus of elasticity in longitudinal direction (GPa)	24.14
	Modulus of elasticity in transverse direction (GPa)	25.25
	Ultimate elongation in longitudinal direction (%)	1.31
	Ultimate elongation in longitudinal direction (%)	1.06
	Ply thickness (mm)	0.66
QuakeBond™ 220UR [54]	Tensile strength (MPa)	38.6
	Flexural strength (MPa)	61.4
	Compressive strength (MPa)	80.7
	Tensile elongation (%)	5
	Full cure time (hours)	12

2.2. Fabrication of GFRP jackets

The GFRP jackets used in this study were fabricated using the continuous flexible PileMedic™ (PLG60.60) GFRP laminate [53] that was wrapped and bonded using a resin material to produce a circular tube around the column. The properties of the laminate and resin according to manufacturers are shown in Table 2. The manufacturer recommends that a minimum wrap of two turns (720 degrees) plus an overlap of 200 mm is to be maintained in the wrapping process. Hence, the laminate sheet was cut in lengths of $2\pi D+200$ where D is the diameter in millimeters for the desired column i.e., 250 mm for the columns CC and 310 mm for columns CC-CM and CC-E. The laminate rolls are provided with a width of 1270 mm which is equal to the length of specimens, so there was no need to cut the sheets in the width direction. The preparation of the GFRP jacket is shown in Fig. 3. Prior to fabrication of jackets, the surface of laminates was wiped clean to remove any contaminants from the surface with consideration taken not to damage the fibres and to maintain the properties of the composite. To construct the jacket, the sheets were firstly cut into the appropriate length out of the long roll. Then, the QuakeBond™ 220UR underwater

resin [54] was mixed according to the procedure described in the product data sheet. During the fabrication of jackets, the first part of the laminate that will be installed against the column does not need to be coated with epoxy, anyhow, the remaining part was coated using a trowel with special care taken to keep the epoxy thickness around 1 mm. Finally, the jackets were left to cure for at least 48 h.

2.3. Instrumentation and test setup

Fig. 4a shows a schematic diagram for the flexural test setup of unwrapped and GFRP-wrapped RC columns under three-point bending. The tests were carried out at the University of Southern Queensland Centre for Future Materials (CFM) engineering laboratory. The bending test was performed over a simply supported beam with clear and shear spans of 1000 mm and 500 mm, respectively. The load was applied monotonically at midspan until failure. Before loading commenced, a neoprene rubber pad of 3 mm thickness was provided under the loading point for all specimens to ensure uniform distribution of loading during the testing and to avoid local indentation failures. The supporting cradles were cut from a hardwood F27 timber piece and formed in a shape to provide a stable supporting system for the tested column. These cradles were firmly tied with steel plates connected to the testing machine using four M12 G8.8 bolts. In order to measure strains during loading, all columns were equipped with a 3 mm single element uniaxial strain gauge (FLAB-3-11-3LJCT-F) affixed to the outer surface of the midspan tension side (surface of concrete for columns UC and surface of GFRP wrap for columns CC-CM and CC-E), where the gauges are oriented in the longitudinal and transverse directions of the columns. All columns were tested up to failure and failure mechanisms were observed and reported.

Columns UC and CC were tested using a 400 kN SANS universal testing machine (Fig. 4b). The specimens were tested under displacement control of 3 mm per minute. Applied loads and corresponding midspan deflections were obtained from the computer system of the testing machine while the strain recordings were obtained using the “System 5000” data acquisition system. Due to the limited capacity of SANS machine and expectations for high failure loads of the GFRP-wrapped specimens with infills, columns CC-CM and CC-E were tested using a 2000 kN structural test frame (Fig. 4c). The applied loads were measured using a 500 kN loading cell and midspan deflections were captured using linear variable displacement transducers (LVDTs). The applied loads, midspan deflections and strains were obtained using a data logger.

2.4. Material properties

2.4.1. GFRP jackets

Fig. 5 depicts the details of the tensile testing performed on longitudinal and transverse GFRP coupons. The tensile tests were conducted on six coupons from each direction to acquire the tensile properties and modulus of elasticity using the MTS universal testing machine (Fig. 5a) with a capacity of 100 kN and a standard head displacement of 2 mm/min. To fabricate the samples, two laminates of PLG60.60 [53] were glued using QuakeBond™ 220UR underwater resin [54]. The selection of this combination was based to simulate the actual composition of the jacket used for the full-scale bending tests. The bonded sheet was left to cure for 7 days before it was cut using a water jet-cutting machine into coupons following the ASTM D3039-17 Standard [55] (Fig. 5a).

In addition, end tabs were cut from the same sheet and bonded to the ends of the tested coupons to provide an adequate gripping area at ends and to prevent slipping. Prior to testing, the measurements of all samples were taken using a micrometer in three different locations of each sample. Also, five coupons from each direction were instrumented in the mid length with a 3 mm uniaxial strain gauge to obtain the full stress

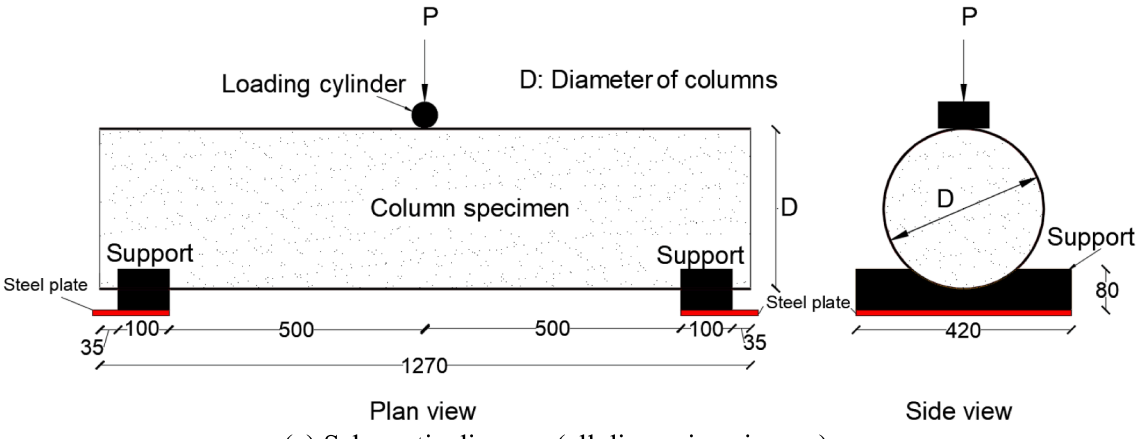

(a) Schematic diagram (all dimensions in mm)

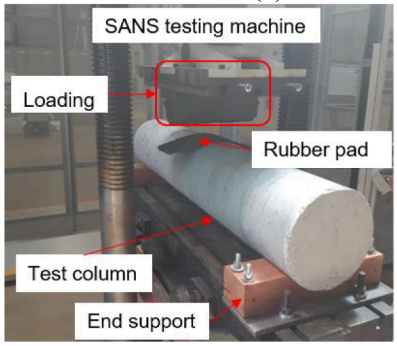

(b) UC and CC

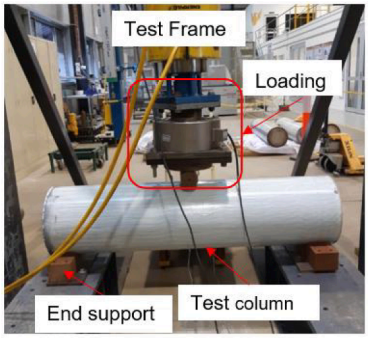

(c) CC-CM and CC-E

Fig. 4. Test setup of full-scale columns.

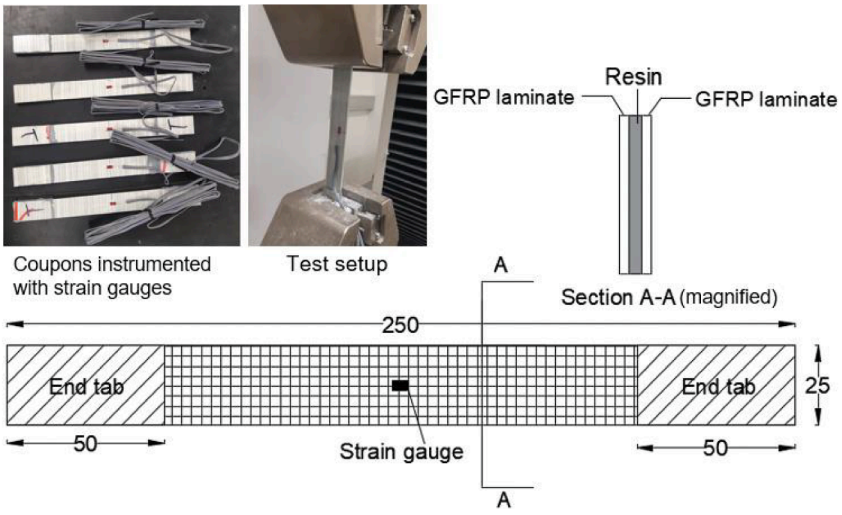

(a) Test setup and details of tensile coupons (all dimensions in mm)

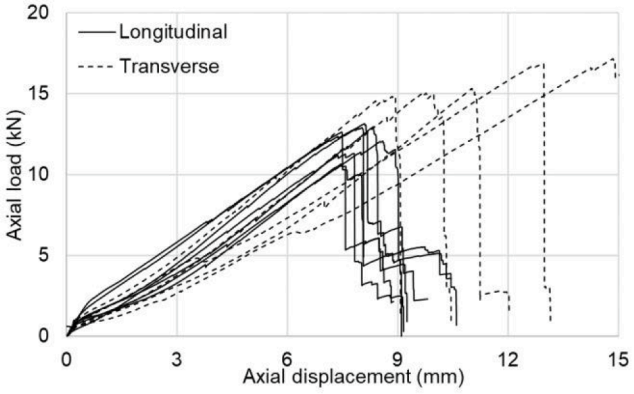

(b) Axial load-displacement curves

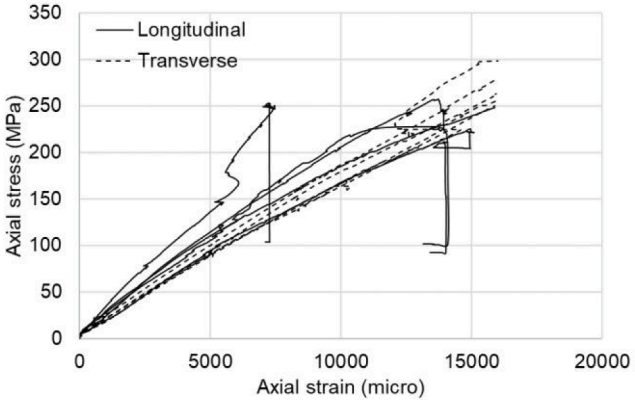

(c) Axial stress-strain curves

Fig. 5. Tensile testing results of GFRP coupons.

strain behaviour. The coupons were property clamped with the jaws of the testing machine to avoid any misalignments and then samples were tested until failure. The load -displacement curves (Fig. 5b) were obtained from the MTS machine while the strain values obtained from the strain gauges were used to plot the stress strain curves (Fig. 5c). The stresses in coupons were obtained by dividing the applied load by the cross-sectional area. The average results of strength and modulus of elasticity are listed in Table 3.

2.4.2. *Concrete, infills and steel reinforcement*

The ready- mix normal strength concrete was provided by a local supplier and used for casting all the specimens. The compressive strength of concrete was determined in accordance with AS1012.9:2014 Standards [56] by testing three concrete cylinders with a diameter of 150 mm and a height of 300 mm. The underwater cementitious grout [57] and the underwater pile jacket epoxy grout [58] were used as infill materials in this study. These materials were selected due to their effective performance in strength and elongation and being commonly used in practice. The underwater cementitious grout is a cement-based grout commonly used for pile restoration and the pile jacket epoxy grout is a three-component underwater structural epoxy consisting of low viscosity resin and a hardener system mixed with aggregate to provide a high strength adhesive which is used to fill the PileMedic jacket systems in concrete and timber substrates. Three cylindrical samples were prepared from the cementitious grout infill with a diameter of 150 mm and a height of 300 mm and tested under compression in accordance with AS1012.9:2014 Standards [56]. The properties of concrete and grout were obtained from a recent research work conducted by authors [38]. In addition, three cylinders of the pile jacket epoxy grout with a diameter of 100 mm and a height of 200 mm were prepared and tested following the similar standards. The properties of

Table 3
Mechanical properties of GFRP jackets.

Property	Longitudinal direction		Transverse direction	
	Average value	Standard deviation	Average value	Standard deviation
Thickness (mm)	1.96	0.05	2.01	0.13
Tensile strength (MPa)	264	24.5	317	34.6
Modulus of elasticity (MPa)	9962	2494	14,132	737

Table 4
Properties of concrete and infills materials.

Material	Property	Value
Concrete	Compressive strength (MPa)	21.7
	Compressive strain at peak	0.0045
	Modulus of elasticity (MPa)	6305
Grout	Compressive strength (MPa)	44.4
	Compressive strain at peak	0.0027
	Modulus of elasticity (MPa)	13,653
Epoxy	Compressive strength (MPa)	88.9
	Compressive strain at peak	0.0215
	Modulus of elasticity (MPa)	5888

concrete and infills materials are listed in Table 4. Furthermore, deformed steel bars [59] with a nominal diameter of 12 mm and a yield strength of 500 MPa were used to reinforce the columns in the longitudinal direction, while undeformed steel bars with a diameter of 8 mm and a yield strength of 250 MPa were used for the transverse reinforcement.

2.4.3. Definition of peak strengthening ratio, yield strengthening ratio, ductility and energy absorption

The strengthening ratios, ductility and energy absorption are important to properly investigate and compare the influence of the wrapping system on the overall flexural performance of RC columns. The deflection at yield load was determined as the deflection at the intersection point of two straight lines. The first line is the best-fit regression line to the linear segment of the load-deflection curve and the second line is the horizontal line passing the peak flexural load point as also implemented by Hadi et al. [16]. The yield load was then determined as the load corresponding to the deflection at yield. The energy absorption was determined as the area under the load- deflection curves and was calculated mathematically from the experimental data over the whole load history. The ductility of RC columns shows their capability to sustain plastic deformations without a significant loss in strength [60] and was determined as the ratio of the deflection at 85% of the peak flexural load in the post peak region to the deflection at the yield [61]. For columns with no descending post peak response, the ductility was computed as the deflection at failure divided by the deflection at yield. The yield strengthening ratio was obtained by dividing the yield load of specimen by yield load of the control column, whereas the peak strengthening ratio was obtained by dividing the peak flexural load of each column by the peak flexural load of the control column. The energy absorption ratio was obtained by dividing the energy absorption of column by energy absorption of the control column and ductility ratio was obtained as the ratio between the ductility of each column and ductility of the control column. It should be noted that the behaviour of column UC1 was considered as a benchmark to compare the performance of tested columns. Additionally, it is worth mentioning that a variety of factors affect the described measurements, including material properties, reinforcing layout, sectional size, and loading type [62–68]. The variety of localised damage, for instance, causes a loss in ductility as the length of the constant-moment zone in a four-point bending beam increases[65]. Therefore, the values presented herein are limited to the properties and dimensions of the investigated columns.

3. Results and observations

This section presents the experimental results and observations in term of failure modes and flexural load-midspan deflection behaviour. It also evaluates the effectiveness and contribution of the GFRP wrapping system to the flexural behaviour of the RC columns.

3.1. Failure modes

Fig. 6 shows the failure modes of tested columns under three-point bending. Columns UC failed by typical vertical flexural cracks in the vicinity of the midspan tension zone. This is attributed to the effect of flexural stresses (Fig. 6a). Fine cracks appeared in the midspan region and as the applied load increased, these cracks widened and propagated upwards to the loading point. At approximately 125 kN, the vertical cracks rapidly widened until the peak load was achieved. Beyond the peak, the columns were observed to sustain large deflection, and this was due to yielding of longitudinal steel reinforcement before final failure caused by concrete crushing in the compression side.

Fig. 6b shows the failure mode of column CC1 which was initiated by formation of localized cracks at the tension side of midspan region. The sound of GFRP localized fracturing could be heard as the load increased while, longitudinal cracks in GFRP started to propagate upwards to the column mid height. At the same time, circumferential cracks at the top region of midspan were observed due to compressive stresses and indicated that there was crushing of the underlying concrete. The final failure occurred due to fracture of GFRP fibres in the longitudinal direction of the midspan tension zone. In contrary, the failure of column CC2 was different from column CC1 as separation of GFRP laminate started at approximately 190 kN. Initially, no appearance of circumferential cracks was observed around the column in the compression zone of midspan region. This indicates that there was no transfer of stresses from the entire concrete to the surrounding wrap. Afterwards, a slight drop in load was observed and associated with dramatic increase in deflection. Meanwhile, separation of the GFRP wrapping was observed and accompanied with circumferential distortion of wrap and slipping out of the concrete column at the end region as shown in Fig. 7. Columns CC-CM (Fig. 6c) and CC-E (Fig. 6d) had similar failure modes to that of column CC1 which was governed by the fracture of GFRP in the longitudinal direction at midspan in the tension side. As the load progressed, localized cracking of GFRP laminate appeared in various locations in the midspan region. After that, cracks in the tension side widened and propagated towards the mid height. In addition, the circumferential cracks formed in the compression side around the

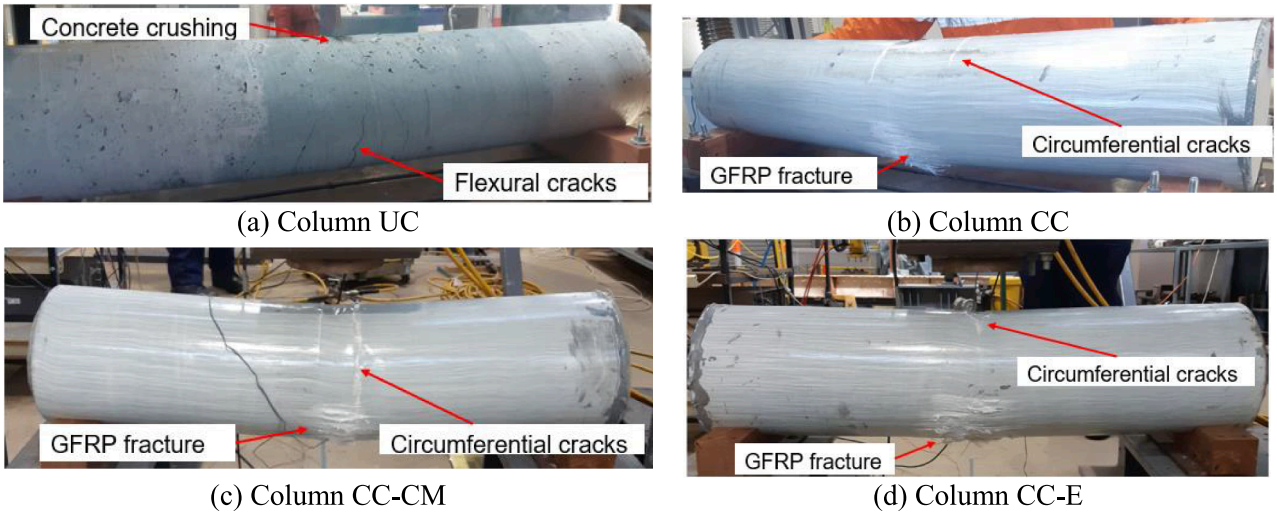

Fig. 6. Failure modes of columns tested under flexure.

Fig. 7. Failure mode of column CC2.

loading point, and these cracks progressed downwards to the column's mid height. The extension of the circumferential cracks in the compression zone illustrates the activation of the GFRP confinement and was mostly observed in columns CC-CM due to crushing of the grout infill beneath the wrap which resulted in exhibiting large midspan deflections compared to other columns.

3.2. Flexural load and midspan deflection behaviour

Fig. 8 depicts the relationship between the experimental flexural load and midspan deflection of tested columns. Table 5 reports a summary of the experimental results of tested columns in terms of peak load, yield load, corresponding deflections, moment capacity, energy absorption and ductility. The ascending load-deflection curves can be described by two different phases. The first phase represents the column behaviour up to the yielding of the longitudinal steel and characterized by a quasi-linear load-deflection response with different stiffness depending on the status of GFRP wrapping. In the second phase, the post yield region showed a slight reduction in stiffness accompanied with an increase in the midspan deflection until the peak load is approached. This is due to widening of tensile cracks in the tested columns. This response is consistent with the test results discussed in a previous study by Pham et al. [31] where the load-deflection curves exhibited a descending response after yield with a variation in slope depending on the compressive strength of the wrapped material. It is evident that columns UC and CC showed similar initial stiffness. This may be attributed to that GFRP wrapping is not contributing to columns behaviour prior to cracking of concrete. However, for columns CC-CM and CC-E, the initial stiffness is apparently larger than those for UC and CC columns. This is due to the increased second moment of area of the wrapped sections with infills, which could enhance the section stiffness and reduce the midspan deflections at the same level of applied

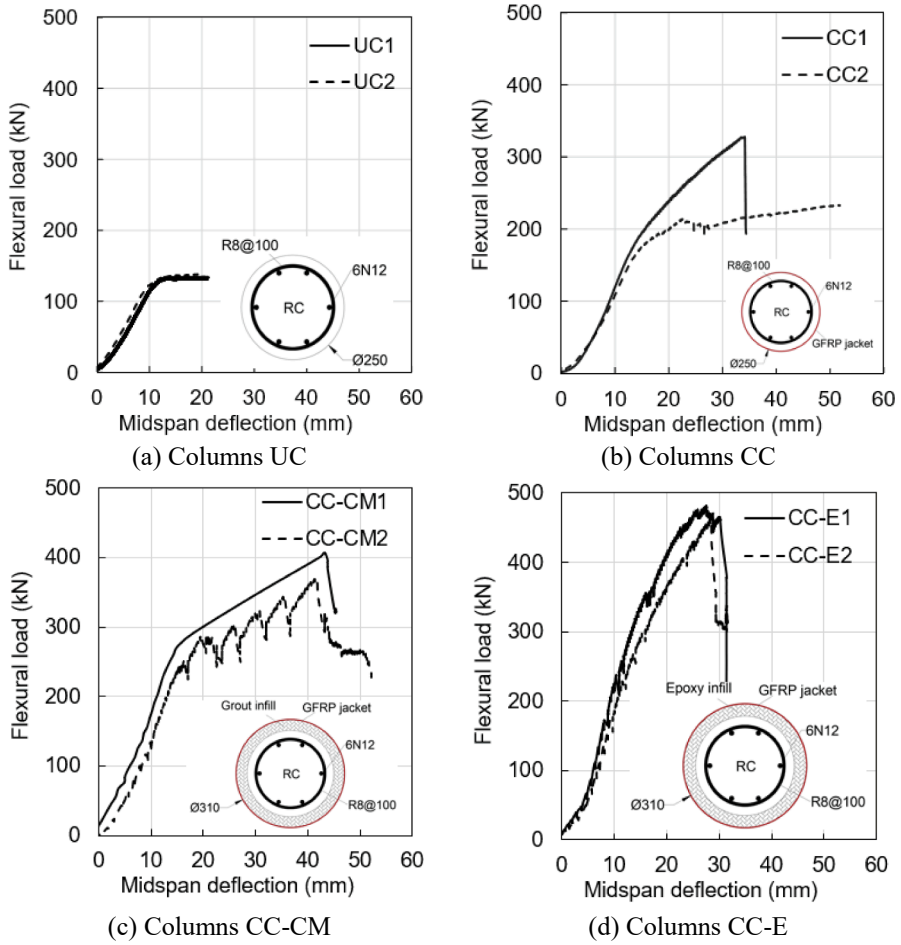

Fig. 8. Experimental load- midspan deflection curves of tested columns*. * *Note: All dimensions in columns' cross sections are in mm.*

Table 5
Experimental results of columns tested under three-point bending.

Column	UC1	UC2	CC1	CC2	CC-CM1	CC-CM2	CC-E1	CC-E2
Peak load (kN)	133	137	328	214	406	369	482	462
Deflection at peak load (mm)	13.9	14.8	34.1	22.5	43.2	41.3	27.5	28.4
Yield load (kN)	131	130	262	191	278	264	431	414
Deflection at yield load (mm)	12.9	12.5	22.9	17.5	18.3	20.5	20.7	24.3
Energy absorption (kN-mm)	1975	1987	6468	9027	12,382	12,421	9242	8113
Ductility	1.64	1.60	1.49	2.96	2.47	2.11	1.48	1.18
Moment capacity (kN-m)	33	34	82	54	102	92	121	116
Peak strengthening ratio	1.00	1.03	2.46	1.61	3.05	2.78	3.62	3.47
Yield strengthening ratio	1.00	0.99	2.00	1.46	2.11	2.01	3.28	3.15
Energy absorption ratio	1.00	0.99	3.28	4.57	6.27	6.29	4.68	4.11
Ductility ratio	1.00	0.98	0.91	1.81	1.51	1.29	0.90	0.72

load. The wrapped columns presented a substantial increase in the flexural load capacity over the unwrapped columns. As summarized in Table 5, columns CC-E achieved the highest peak flexural load. The GFRP wrapping system increased the flexural load capacity to an average of 271 kN, 388 kN and 472 kN for columns CC, CC-CM and CC-E, respectively corresponding to an enhanced flexural moment capacity of 101%, 187% and 249%, respectively. This shows that the GFRP wrapping system has an effective contribution to the flexural strength.

The average yield load for columns UC (Fig. 8a) was 131 kN with corresponding midspan deflection of 12.7 mm. The post yield showed a hardening response up to an average peak load of 135 kN with corresponding deflection of 14.4 mm. Subsequently, the post peak response showed an approximately constant load until failure at a deflection of 20.6 mm. This plateau behaviour is attributed to yielding of longitudinal steel reinforcement. The average energy absorption and ductility of columns UC were 1981 kN-mm and 1.62, respectively.

Columns CC (Fig. 8b) showed a different behaviour compared to columns UC, in particular, for the post yield response. Column CC1 had a quasi-linear response up to 200 kN, afterwards, the stiffness of column started to decrease slightly until achieving the peak load of 328 kN with a corresponding deflection of 34.1 mm. In the post peak, the load dropped suddenly to 194 kN causing the final failure. In comparison with UC1, column CC1 sustained an increase of 147% and 146% in peak load and corresponding deflection, respectively. This implies that GFRP wrapping imparted additional external reinforcement that enhanced the flexural behaviour of the wrapped column. The inclusion of GFRP wrap in column sections allows to provide more tensile and compressive forces and hence increase the flexural moment capacity in order to achieve equilibrium of internal forces. Moreover, the yield load of column CC1 increased by 100% compared to UC columns as shown in Table 5. This is attributed to the increased flexural capacity of the RC section due to wrapping and thus a higher load is expected to attain yielding of steel reinforcing bars. Since GFRP wrap has similar distribution of fibres in longitudinal and transverse directions, more stabilization for the internal RC column in the compression zone could occur due to confining pressure exerted by jackets which provides higher resistance to the lateral expansion of concrete under the effect of compression stresses. This also restricts cracks widening until failure of the wraps.

The load-deflection behaviour of column CC2 showed a lower initial stiffness compared to column CC1 and sustained a peak flexural load of 214 kN with corresponding deflection of 22.5 mm. This corresponds to a reduction of 35% and 34% in peak flexural load and corresponding deflection, respectively, compared to column CC1. This can be attributed to the separation of GFRP laminates in the compression zone which also resulted in a hardening response in the post peak behaviour until failure at a deflection of 51.8 mm. The separation of the top GFRP laminates was due to crushing of concrete beneath the wrap which caused failure of the interface between the wrap and concrete. With increased loading, buckling and distortion of wraps was noted in the circumferential direction of the top compression region adjacent to the loading point as can be seen in Fig. 7. Noticeable increase in load carrying capacity was then observed until failure at 232 kN. Hence, the loss of bond with the GFRP wrap in compression region can remarkably affect the overall behaviour of the wrapped columns. This was apparent in the stiffness reduction of column CC2 as shown in Fig. 8b. The post peak behaviour experienced large deflections, and this resulted in an increase of 40% in the energy absorption of column CC2 to achieve 9027 kN-mm compared to 6468 kN-mm for column CC1. Also, it resulted in that column CC2 exhibited a higher ductility ratio than column CC1.

The initial flexural load- midspan deflection curve of columns CC-CM (Fig. 8c) was relatively steeper than that for CC1. Column CC-CM1 showed a peak flexural load of 406 kN which was subsequently, followed by a gradual descending response until failure at midspan deflection of 45.3 mm. The peak flexural load capacity and corresponding deflection significantly increased by 205% and 211%, respectively. This increase reflects that the grout infill and GFRP wrapping improved the behaviour of the RC columns due to its contribution in restricting and delaying the formation of cracks of the entire concrete core. Moreover, the flexural load –midspan deflection curve of column CC-CM2 showed a fluctuated response with frequent drops in the post yield region. This could be attributed to widening of cracks and consequent crushing of the entire grout infill. It is evident that columns CC-CM exhibited the highest energy absorption and ductility ratios with an average of 6.28 and 1.4, respectively. The high ductility values reflect the gain of using grout infills in improving the post peak behaviour of GFRP-wrapped RC columns and achieving high midspan deflections at failure compared to other columns. It could be noted that the yield loads and corresponding deflections of columns CC-CM are very close to that of column CC. This indicates that early crushing of grout infills occurs, however, the post yield response of columns CC-CM are characterised by an enhanced ductile behaviour.

The initial curve of the flexural load –midspan deflection of columns CC-E (Fig. 8d) was the steepest among all tested columns and this shows their high initial stiffness. Columns CC-E reported the highest peak flexural load with an average of 472 kN with a corresponding average midspan deflection of 28.0 mm. Therefore, the provision of epoxy infill material within the GFRP wrapping system can substantially enhance the flexural capacity of RC columns. The average yield load was 57% higher than the yield load of columns CC-CM. Nonetheless, the post peak response was characterised by a sudden drop to failure. In contrast to columns CC-CM, columns CC-E sustained 22% higher peak flexural load and 34% lower midspan deflection. The reduction in the midspan deflection and not undergoing frequent load drops could be attributed to the increased rigidity and brittleness of the epoxy infill associated with the increased compressive strength and corresponding strain compared to the grout infill. The epoxy infill is characterized by strain at peak of 2.15% which is eight times higher than that for grout infills. This accords with Mohammed et al. [42] in terms of that increasing the compressive strength of infill can delay its cracking and degradation. Nevertheless, the reduction in midspan deflection of CC-E columns explains the reason that CC-E columns reported the lowest ductility ratio among all columns

with an average of 0.81 as shown in Table 5, which is 42% lower than that of columns CC-CM, and this points out the less ductile behaviour of GFRP-wrapped columns filled with epoxy

In the experimental results, it is noted that the peak loads of duplicated columns are slightly different by 10% and 4% for columns CC-CM and CC-E, respectively. This discrepancy can be attributed to a variety of reasons including testing setups, minor changes in infill thickness, and the composite behaviour of such structures, which is distinctive due to the inclusion of various constituent materials. Additionally, as seen in Table 5, columns with infills have a significantly higher peak strengthening ratio than columns with no infills. The average increases for columns CC-E and CC-CM were 255% and 192%, respectively, compared to 104% for columns CC. This is to be expected, as the presence of infills can increase the flexural loading capacity of columns by increasing their cross-sectional area. To further emphasise the effect of the cross-sectional area, the average peak loads of tested columns divided by their corresponding cross-sectional areas (P/A) were normalized in comparison to the average value of columns UC, as shown in Fig. 9. The normalized P/A of columns CC-E was found to be 127% higher than that of unwrapped columns, compared to 87% and 101% for columns CC-CM and CC, respectively. The early crushing of grout infill due to its low peak strain could be the reason for the loss of strength in these columns. The loss of bond could have a substantial impact on the GFRP contribution to column capacity due to decreasing stress transfer within the structure.

The effect of enlarged cross section due to infills can be evaluated using Eq. (1) by obtaining the maximum elastic bending stress (f) experienced by the tested columns at same applied moment considering the linear elastic stress theory based on the properties of the uncracked cross- section.

$$f = Mc/I_{uncracked} \tag{1}$$

where M is the bending moment, $I_{uncracked}$ is the second moment of area of the uncracked cross-section about the centroidal axis and c is the distance from the extreme top or bottom fibre of the cross-section to the centroidal axis. The second moment of area is then computed as Eq. (2).

$$I_{uncracked} = I_c + n_f I_f + (n_S - 1)I_S + n_{GFRP} I_{GFRP} \tag{2}$$

where I_c, I_f, I_s and I_{GFRP} are the second moment of area about the centroidal axis of concrete, infill, steel and GFRP, respectively, which can be calculated using Eqs. (3), (4), (5) and (6), respectively.

$$I_c = \pi D_c^4/64 \tag{3}$$

$$I_f = \pi((D_c + 2t_f)^4 - D_c^4)/64 \tag{4}$$

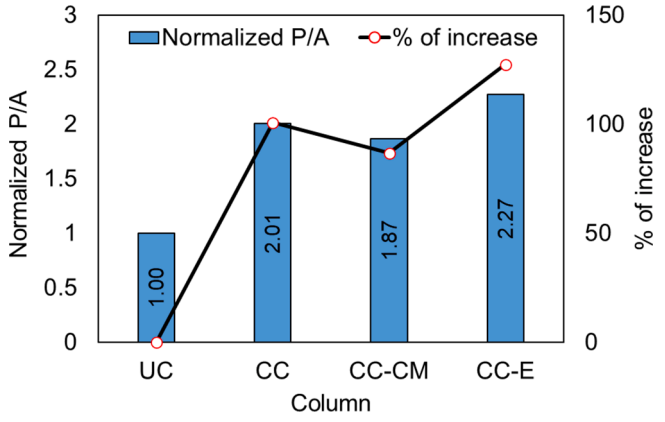

Fig. 9. Normalized P/A of tested columns and corresponding percentage of increase.

$$I_s = \sum_{i=1}^{6} A_{si} y_i^2 \tag{5}$$

$$I_{GFRP} = \pi((D_c + 2t_f + 2t_{GFRP})^4 - (D_c + 2t_f)^4)/64 \tag{6}$$

where D_c is the diameter of the concrete core,t_f and t_{GFRP} are the thicknesses of infill and GFRP jacket, respectively, A_{si} and y_i are the area of each steel bar and its corresponding distance from the centroidal axis of the cross section, respectively as shown in Fig. 10a. The modular ratios are computed using the modulus of elasticity (E) of each material as $n_f = E_f/E_c$, $n_s = E_s/E_c$, and $n_{GFRP} = E_{GFRP}/E_c$ for infill, steel, and GFRP, respectively. It should be noted that the modulus of GFRP in the longitudinal direction was taken in these calculations. It is evident that the increase in the second moment of area of column's uncracked cross section due to enlarged cross section leads to an apparent reduction in the normalised bending stress by approximately 63% and 42% for columns CC-CM and CC-E, respectively in contrast to the unwrapped columns as shown in Fig. 10b. Hence it is clear that the enlarged sections due to the presence of infills, could reveal a dominant reduction in the induced bending stresses in the elastic behaviour.

3.3. *Effect of GFRP wrapping on flexural load versus longitudinal and transverse strains*

Fig. 11 shows the experimental flexural load versus longitudinal and transverse strain curves developed on the tension side in the vicinity of midspan region of tested columns. For columns UC (Fig. 11a), a quasi-linear response was observed up to the peak load followed by a constant load response with increasing strains up to failure. Apart from the unexpected separation failure of columns CC2, all tested GFRP-wrapped columns exhibited large longitudinal strains at failure during the experimental work. Column CC1 (Fig. 11b) showed relatively low longitudinal strains up to a flexural load of 50 kN followed by a dramatic increase until a flexural load of 317 kN with corresponding strain of 15,926 microstrains. Furthermore, no considerable longitudinal strains were reported in column CC2 up to a flexural load of 150 kN, after which, a slight increase occurred in the strains to achieve a longitudinal strain of 4557 microstrains at peak load of 214 kN. The post peak behaviour showed a hardening response up to failure. Columns CC-CM (Fig. 11c) showed similar initial response compared to column CC1 up to an applied load of 80 kN whereas, a sudden drop occurred in the load followed by a slight increase in longitudinal strain up to a load of 264 kN with corresponding strain of 4500 microstrains. Subsequently, the behaviour displayed an ascending response up to 321 kN and 16,285 microstrains and no strains were reported beyond this point. For columns CC-E (Fig. 11d), the stiffer response is observable compared to columns CC-CM which is due to its high tensile strength. However, the strain kept increasing with the applied load until approximately 400 kN and corresponding strain of 16,250 microstrains where the strain gauge damaged and failed to record the strains. The above results demonstrate that the GFRP wrapping can considerably increase the capability of columns to undergo large longitudinal strains in contrast to the counterpart unwrapped columns.

In general, the transverse strains in the circumferential direction reported low values for all tested columns indicating low GFRP confinement efficiency in the tension side. However, in column CC2, the transverse strains increased excessively after a flexural load of 190 kN to achieve 10,795 microstrains at failure. This is attributed to the separation that occurred in the GFRP wrap and unexpected failure mode as shown in Fig. 7.

4. Finite element modelling (FEM)

The experimental program and results give valuable assessment about the contribution of the GFRP wrapping system to the flexural

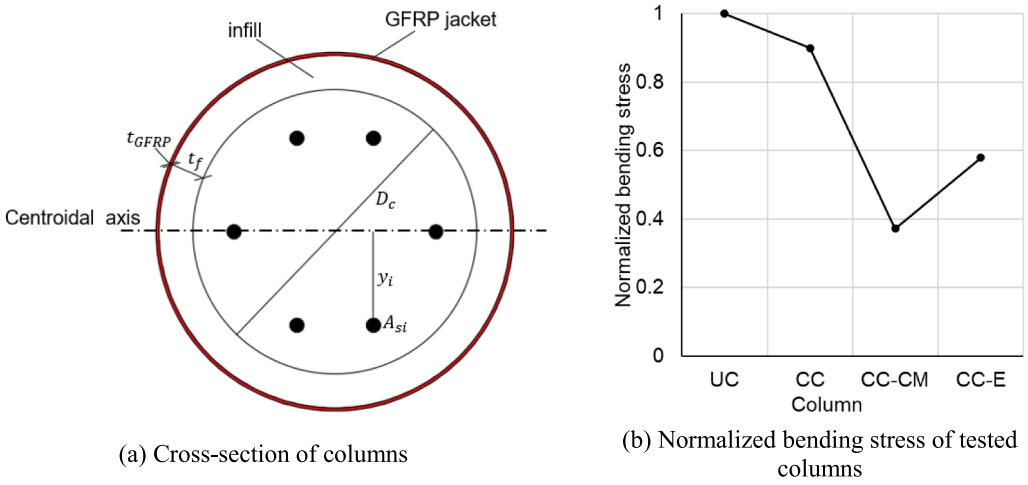

(a) Cross-section of columns (b) Normalized bending stress of tested columns

Fig. 10. Effect of enlarged sections due to GFRP wrapping system.

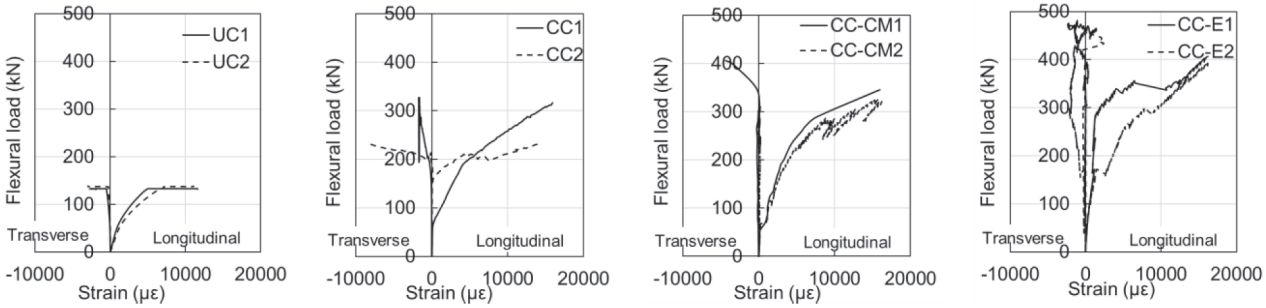

(a) Columns UC (b) Columns CC (c) Columns CC-CM (d) Columns CC-E

Fig. 11. Experimental flexural load- strain curves of the tested columns.

capacity of the RC columns. It is important to further highlight this behaviour numerically to verify the test results and to investigate the influence of this type of wrapping systems on the overall flexural behaviour. The objective of FEM analysis is to obtain comprehensive results that show the overall response of various structures. Such analysis is mostly preferred over standard analytical approaches because of the wide range of findings that can clearly demonstrate the behaviour of various materials compositions and simulate the local impacts of loads on different portions of the structure.

4.1. Development of finite element models

A three-dimensional FEM was developed using various types of elements to represent the variety of the constituent materials. A nonlinear static analysis was conducted in ABAQUS finite element software package [69] to consider the nonlinear behaviour of concrete and infill materials, and to simulate and predict the flexural load- midspan deflection response of the unwrapped and GFRP-wrapped columns under the effect of the three point bending. Initially, the quality of the model was assessed and validated with experimental results of unwrapped columns. After that, the models were extended to accommodate the GFRP-wrapped columns. The accuracy of this model is validated by comparing the FEM results with the experimental results.

4.2. Materials behaviour

4.2.1. Concrete and infill materials

To have accurate FEM predictions, it is important to assign the proper behaviour of the constituent materials. The elastic and plastic behaviour of concrete and infill properties were considered with data provided in Table 4. Poisson's ratios were assumed to be 0.2, 0.2 and 0.18 for concrete, grout and epoxy, respectively. In ABAQUS, the total strain (ε) is divided into elastic strain (ε^{el}) and plastic strain (ε^{pl}) according to the elastoplastic principles. The elastic behaviour is defined by Poisson's ratio and modulus of elasticity (E_o). This behaviour undergoes linear stress-strain response up to an initial value (σ_{co}) for compression and (σ_{to}) for tension which are the peak elastic stresses. The inelastic behaviour of concrete and infill materials under compression and tension loading were represented by the concrete damaged plasticity (CDP) model and obtained using Eqs. (7) and (8) for compression and tension, respectively.

$$\sigma_c = (1 - d_c)E_0(\varepsilon_c - \varepsilon_c^{pl}) \tag{7}$$

$$\sigma_t = (1 - d_t)E_0(\varepsilon_t - \varepsilon_t^{pl}) \tag{8}$$

where d_c and d_t are the damage parameters in compression and tension, respectively. The damage is characterized by the degradation of stiffness and damage parameters in both compression and tension are determined using Eqs. (9) and (10), respectively. These parameters can take values starting from zero for undamaged material up to one representing the fully damaged or loss of strength.

$$d_c = 1 - (\sigma_c/\sigma_{cu}) \tag{9}$$

$$d_t = 1 - (\sigma_t/\sigma_{t0}) \tag{10}$$

where σ_{cu} and σ_{t0} are the ultimate compressive stress and tensile cracking stress of the modelled material, respectively. The CDP model assumes two main failure mechanisms which are tensile cracking and compression crushing of the material. Under uniaxial compression, the

compression inelastic behaviour is divided into two main phases. The first phase starts beyond the elastic behaviour and considers a strain hardening response up to ultimate stress (σ_{cu}) followed by the second phase with a strain softening response up to failure. Under uniaxial tension, the response is assumed as linear elastic up to cracking stress (σ_{t0}) where there would be the formation of tensile cracks. After the crack initiation, a softening post peak response is assumed until failure. In this study, the tension stiffening model proposed by Massicotte et al. [70] was employed to define the post peak tensile behaviour. Although no tensile tests were carried out to determine the tensile behaviour of the constitutive materials, the mean characteristic values of the uniaxial tensile strength of concrete and grout were obtained to be 2.4 and 3.4 MPa, respectively as per AS3600-2009 Standards [52]. Also, a tensile strength value of 12.7 MPa was incorporated for the epoxy infill as provided by the manufacturer. Additionally, in the CDP model, five obligatory parameters are required for defining the plastic behaviour including dilation angle (ψ), eccentricity (e), the ratio of initial biaxial compressive yield stress to initial uniaxial compressive yield stress (f_{b0}/f_{c0}), the ratio of the second stress invariant on the tensile meridian to that on the compressive meridian (K) and Viscosity parameter (μ). The first four parameters were left default as 31 degrees, 0.1, 1.16 and 0.667, respectively, while the viscosity parameter was assigned to be 0.0005 (close to the default zero value) to allow for better convergence. The nonlinear stress-strain (σ-ε) curve of the unwrapped concrete was based on the empirical parabolic relationship given by Warner et al. [71] as shown in Eq. (11).

$$\sigma = \sigma_0\left(\frac{2\varepsilon}{\varepsilon_0} - \left(\frac{\varepsilon}{\varepsilon_0}\right)^2\right) \tag{11}$$

where σ_0 and ε_0 are the unwrapped concrete peak axial stress and corresponding strain, respectively. However, for grout and epoxy infills, the actual material compressive properties obtained from the experimental tests were incorporated into the FEM simulation. Furthermore, the timber cradles used to support the columns in this testing program were assumed to have a modulus of elasticity and Poisson's ratio of 18 GPa and 0.48, respectively as per AS 1720.1-2010 Standards [72].

4.2.2. Steel reinforcement

The behaviour of longitudinal and transverse reinforcement was represented by a bilinear elastoplastic constitutive relationship with linear strain hardening. This behaviour undergoes elastic response up to the yield stress while any further loading will produce plastic strains. The modulus of elasticity and Poisson's ratio were taken to be 200 GPa and 0.3, respectively. The plastic behaviour was defined so that plasticity of reinforcement occurs upon the achievement of yield strength.

4.2.3. GFRP composite

The elastic behaviour of the GFRP composites was defined using orthotropic elasticity in plane stress, where only the values of E_1, E_2,υ_{12}, G_{12}, G_{13} and G_{23} are required to define an orthotropic material [69] and the out of plane stress is taken as zero. These values are listed in Table 6. The values of the tensile moduli are based on the experimental results performed on the GFRP coupons and detailed in Section 2.4.1, while the Poisson's ratio and shear moduli were obtained from Kaya et al. [14] where the same type of GFRP was used. It should be noted that in the wrapping process, the longitudinal direction of laminates was oriented with the circumferential direction of columns.

Hashin damage criterion [73] available in ABAQUS was incorporated in this study to model the damage initiation of GFRP composite. The tensile properties obtained from coupon testing were used herein while other strength properties were defined to match the FEM predictions with experiments. After the initiation of damage, degradation of the stiffness occurs with the application of loading. However, the damage evolution response requires the definition of the fracture energy in both the fibre and normal directions. This value was assumed to be 100 N/mm to model GFRP composites. In most cases, the fracture energy values do not need to be at high level of accuracy to obtain accurate FEM results [74]. Also, a value of 0.001 was assigned to be the viscosity coefficient for each failure mode of the GFRP composite as recommended by ABAQUS. The different parameters used to define the Hashin model for the GFRP jacket are presented in Table 7.

Table 6
Elastic properties of GFRP.

Property	Parameter	Value
Elastic properties	Tensile modulus in circumferential direction (E_1) (MPa)	9962
	Tensile modulus in longitudinal direction (E_2) (MPa)	14,132
	Poisson's ratio (υ_{12})	0.28
	Shear moduli, G_{12}, G_{13}, G_{23} (MPa)	1731

4.3. Mesh discretization and boundary conditions

4.3.1. Model geometry and meshing

Appropriate geometrical and meshing elements were used to represent the model of constituent materials. The concrete, infill and supporting jigs were modelled using three-dimensional deformable solids and meshed by 8-node hexahedral elements with reduced integration (C3D8R) and hourglass control. The longitudinal reinforcement was simulated as three-dimensional wire and meshed using 2-node linear three-dimensional truss elements (T3D2). It has been noted that truss elements are more compatible than beam elements for modelling reinforcement bars due to accuracy of results and less computational time [75]. The transverse reinforcement was modelled by three-dimensional deformable solid elements to be able to create the spiral shape. Furthermore, the GFRP jackets were simulated using a three-dimensional deformable shell and meshed by 4-node doubly curved shell elements with reduced integration (S4R) and hourglass control. The loading cylinder was modelled as a three-dimensional rigid part and meshed by 4-node bilinear rigid quadrilateral elements (R3D4). The constituent elements of a rigid body do not deform but can undergo large motions and R3D4 elements are used to model the two-dimensional surfaces of a three-dimensional rigid body [69]. Several researchers have employed rigid bodies in simulating the loading application using various testing setups [76–79]. Therefore, the loading cylinder was first created as a discrete rigid part with solid shape before incorporating a shell-from-solid feature using the *shape* option in ABAQUS. The geometry and meshing details of the FEM are shown in Fig. 12.

4.3.2. Interactions and boundary conditions

The coordinate system of the columns was defined as the cross-section plane lays in the global X-Y plane and the longitudinal direction of columns was aligned along the global Z-axis. To determine the load-deflection behaviour up to failure of columns, a static monotonic loading was applied on the top loading cylinder by the displacement-controlled technique. To apply this boundary conditions, a reference point was assigned on top of the loading cylinder to induce this displacement as the motion of this point governs the motion of the rigid body [69]. Also, the bottom face of supports was restrained in all directions (ENCASTE) to simulate the actual experimental work.

Table 7
GFRP strength variables of Hashin model.

Property	Parameter	Value
Strength properties	Tensile strength in circumferential direction (MPa)	264
	Tensile strength in longitudinal direction (MPa)	317
	Compressive strength in circumferential direction (MPa)	150
	Compressive strength in longitudinal direction (MPa)	150
	Shear strength (MPa)	50

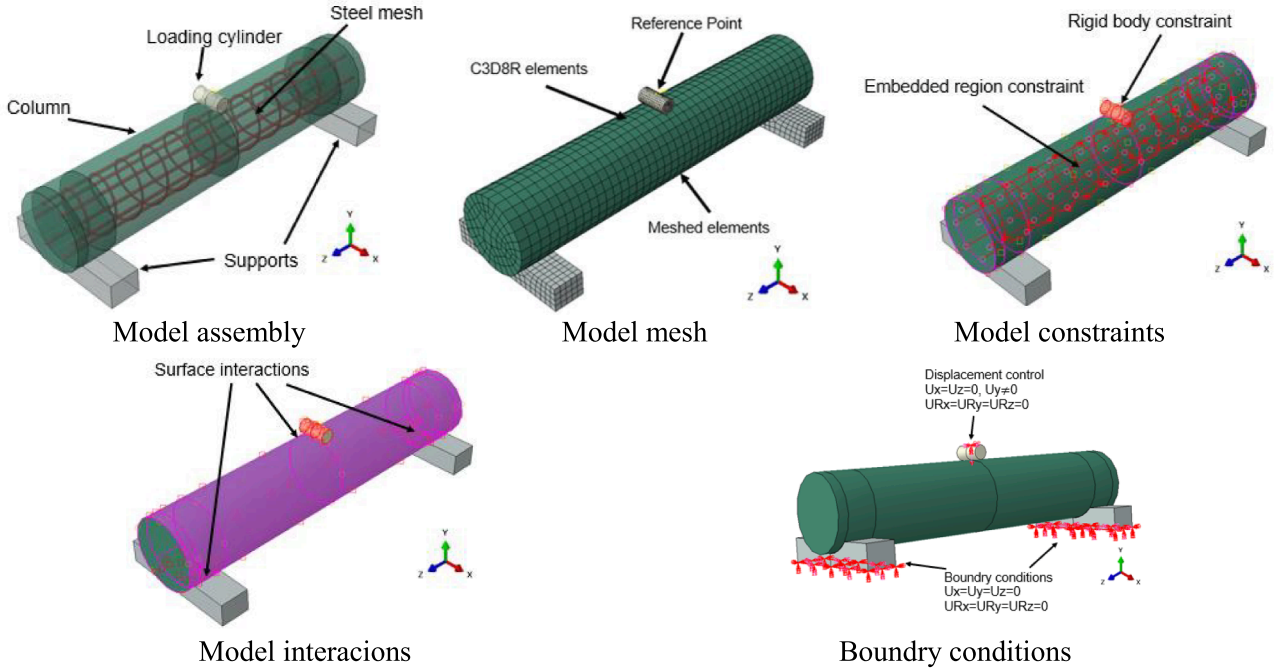

Fig. 12. Details of ABAQUS Model.

Moreover, different interactions were assumed to define the connection of the different parts of the model. The motion of the loading cylinder was constrained with the reference point by providing a rigid body constraint. Additionally, the embedded region constraint was utilized to simulate the bond between the steel reinforcement and the "host" concrete region assuming perfect bond. The interactions between the surfaces of concrete, infill and GFRP were modelled following two different approaches. In the first approach, tie constraints (referred as FEM-1 hereinafter) were used to simulate the contact surface between the elements of parts assuming perfect bond. In the second approach, the contact between concrete, infill and GFRP surfaces was simulated using a surface to surface normal and tangential interaction (referred as FEM-2 hereinafter) with a friction penalty of 0.3 assigned for the coefficient of friction while a "Hard" contact was defined in the normal interaction between surfaces to allow for the separation of contacted surfaces with no penetration. Similarly, surface to surface interaction was assumed between the column and both the loading and supporting elements. The model interactions and boundary conditions are presented in Fig. 12.

4.3.3. Model verification

The experimental results of the unwrapped columns UC1 and UC2 were employed to calibrate and validate the FEM predictions. The time increment step was kept automatic, and initial and maximum increment sizes were kept as 0.01 throughout the analysis. The sensitivity analysis of the load-midspan deflection due to the variation of the mesh size was performed to select an appropriate mesh size for the entire model as shown in Fig. 13.

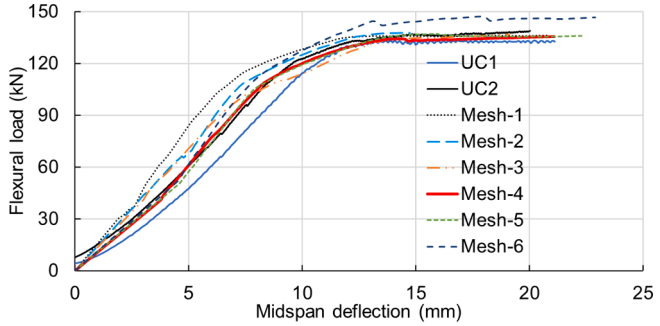

Fig. 13. Mesh sensitivity analysis.

A convergence of results is achieved when the increase in the mesh elements has a negligible effect on the results with considerations taken to match with experimental results and to reduce the computation time. Six different mesh configurations were established in the analysis of the unwrapped column to investigate the mesh sensitivity of the model. It can be noted that the FEM predictions give similar results in terms of the peak load and corresponding midspan deflections except for the model of mesh-6 which showed a maximum variation of 9%. After all, the model with mesh-4 configuration yielded the closest results to the experimental results and therefore was considered for this study.

4.4. FEM results and comparisons with the experiments

4.4.1. Effect of GFRP wrapping system on load- midspan deflection

Fig. 14 depicts the experimental and FEM analysis results of flexural load versus the midspan deflection and shows that there is a good comparison between the FEM and experimental data. Table 8 summarizes the experimental and FEM peak loads (P_{peak}) and corresponding midspan deflections (Δ_{peak}) for the tested columns. The results demonstrate that the experimental peak flexural load and midspan deflection for columns UC (Fig. 14a) are well corresponded with the predicted FEM results with a maximum difference of 3.2%. The FEM prediction for columns CC (Fig. 14b) using the first approach (FEM-1) was well correlated with the experimental performance of column CC1 and achieved a peak load of 319 kN with a corresponding midspan deflection of 33.0 mm as shown in Table 8. The experimental results slightly overestimate the FEM predictions for the peak flexural load and its corresponding deflection by 2.9 and 3.5%, respectively. This indicates that the assumption of using tie constraints adopted for the first approach was accurate in simulating the contact interaction between concrete and GFRP wrap. On the other hand, the second approach (FEM-2) which allows for the separation of GFRP wrap has a close match with the experimental load-displacement curve of the column CC2. This accords with the observed separation of GFRP after a flexural load of approximately 190 kN. The FEM predictions (FEM-2) indicated a peak flexural

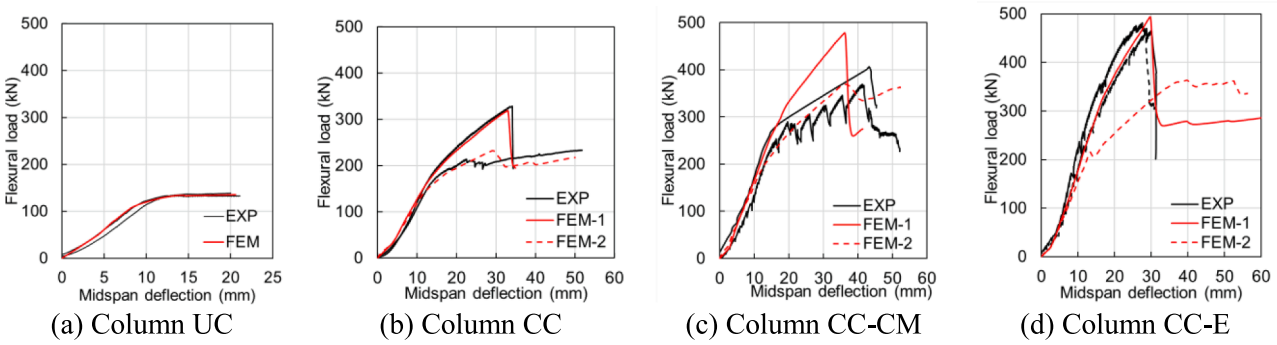

Fig. 14. Experimental and FEM flexural load- midspan deflection curves.

Table 8
Average experimental and FEM results of peak flexural load and corresponding midspan deflection.*

Column	P_{peak} (kN)					Δ_{peak}(mm)				
	P_{EXP}	P_{FEM-1}	P_{FEM-2}	$\frac{P_{EXP}}{P_{FEM-1}}$	$\frac{P_{EXP}}{P_{FEM-2}}$	Δ_{EXP}	Δ_{FEM-1}	Δ_{FEM-2}	$\frac{\Delta_{EXP}}{\Delta_{FEM-1}}$	$\frac{\Delta_{EXP}}{\Delta_{FEM-2}}$
UC1	133	134		0.991		13.9	14.4		0.968	
UC2	137			1.021		14.8			1.030	
CC1	328	319	232	1.029	1.414	34.1	33.0	29.1	1.035	1.174
CC2	214			0.671	0.922	22.5		29.1	0.683	0.775
CC-CM1	406	479	369	0.848	1.099	43.2	36.2	36.3	1.195	1.189
CC-CM2	369			0.771	0.999	41.3		36.3	1.142	1.136
CC-E1	482	494	364	0.975	1.325	27.5	29.7	39.7	0.926	0.693
CC-E2	462			0.935	1.270	28.4		39.7	0.956	0.716

* Note: UC columns have only one FEM result as there is no wrapping system in these columns.

of 232 kN compared to 214 kN reported by the experiment, however, this elaborates a concern about the bond behaviour between this type of wrap and concrete substrate. Fig. 14c presents the FEM results of columns CC-CM and proves that assuming a surface-to-surface contact (FEM-2) between the GFRP wrap, grout infill and concrete, yielded a peak flexural load of 369 kN which is only 10% lower than the experimental result obtained for column CC-CM1 and the same as the peak load noted for column CC-CM2. Although a good correlation is obtained in predicting the peak flexural load, the predicted midspan deflection at peak load is not well corresponded with the experimental results. The slight differences between the proposed FEM and the testing results may be attributed to the variance between the real and the numerical circumstances, discrepancy in material properties and the assumptions made to simulate the surface-to-surface interactions between concrete, grout infill and GFRP wrap. Nevertheless, the assumption of having tie constraints (FEM-1) for column CC-CM shows a high discrepancy which reached 23% between the experimental and FEM results, indicating that the assumption of having a perfect bond between the grout infill and both the substrate concrete and the surrounding GFRP wrap may not be realistic.

The predicted response of columns CC-E (FEM-1) (Fig. 14d) is characterized by a perfectly linear performance up to a flexural load of 314 kN whereas a slight drop occurred in the curve slope due to yielding of steel reinforcement. Thereafter, a good match with the experimental curve is observed until achieving the peak load at 494 kN which is only 4.5% higher than the average peak load obtained by experiments. Moreover, Table 8 shows that a good correlation exists in columns CC-E for predicting the midspan deflection at peak flexural load with an average ratio of 0.94 between the experimental and FEM deflection results. This well-matched model assumes a perfect contact between concrete, epoxy and GFRP wrap, however, the model that considers surface-to-surface interactions (FEM-2) showed a diverse relation compared to experiment. This implies that the perfect bond between epoxy infill and both the concrete substrate and the surrounding GFRP wrap could be considered to represent the real behaviour. Finally, it should be noted that the results of models which have been found to best fit with experiments are used in the discussion presented in the following Section 4.4.2.

4.4.2. Effect of GFRP wrapping system on longitudinal strains of steel bars and failure modes

The performance of the internal steel bars is crucial and must be considered in the analysis to further understand its effect on the overall flexural performance of RC columns and failure mechanisms. Fig. 15 presents the FEM results for the flexural load-strain behaviour of longitudinal steel bars in the vicinity of midspan region of simulated columns. This region displayed the highest tensile and compressive strains in the bottom and top longitudinal bars, respectively. The results of the bar elements which exhibited the highest strain values were selected to plot the strain curves presented in Fig. 15.

Additionally, the FEM predicted yield load and strains at peak flexural loads of tensile and compressive steel reinforcement are presented in Table 9. It is worth noting that according to the material properties of steel bars, the yielding strain for the longitudinal steel is 2500 micro-strains. It is observed that in all columns, longitudinal tensile bars yielded before the peak load. However, the yield loads and post yield responses remarkably vary according to the type of GFRP wrapping system and infill material. The predicted initial load-strain response of columns CC-E showed the highest stiffness among the modelled columns and this could be attributed to the high rigidity of the epoxy material compared to concrete and grout materials as this can delay the transfer of stresses to the internal steel reinforcement and thus delaying the yield of steel bars.

It is evident that columns UC revealed the lowest yield load of 105 kN compared to other columns, nonetheless, the top reinforcement yielded immediately after the peak load and this could be due to high stresses in concrete compression zone. The failure of column UC occurred due to yielding of longitudinal bottom steel followed by concrete crushing in the top compression zone. Interestingly, the simulated model of column CC (FEM-1) is the only model which showed that top longitudinal steel

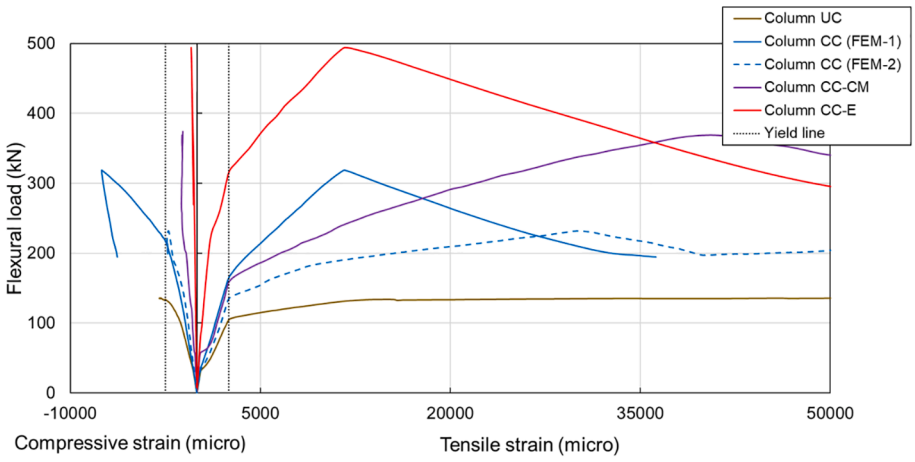

Fig. 15. Predicted flexural load-strain behaviour of longitudinal steel bars at midspan.

Table 9
Predicted yield loads and strains of tensile steel reinforcement at peak load.

Column	Tensile reinforcement		Compressive reinforcement	
	Yield load (kN)	Strain at peak (micro)	Yield load (kN)	Strain at peak (micro)
UC	105	15,218	133	−2487
CC (FEM-1)	167	11,633	219	−7530
CC (FEM-2)	133	29,928	-*	−2248
CC-CM	159	40,565	-*	−1167
CC-E	314	11,743	-*	−448

* Note: No yielding was reported for the top reinforcement.

could undergo a substantial yielding response to achieve the maximum compression strain of 7530 microstrains at peak. In addition, the FEM simulation of columns CC (FEM-1) showed that at a flexural load of 167 kN, the longitudinal tensile steel approached yielding whereas after that, the load-strain curve showed a slight reduction in stiffness until reaching peak load at 11,633 microstrains. It is also well observed that beyond the yield point, column CC could sustain higher loads than column UC which showed a constant load-strain response. This points out the effectiveness of GFRP wrapping as an external reinforcement in utilizing the capability of the internal tensile bars to work adequately and sustain high strains after yielding. Fig. 16 and Fig. 17a presents the tensile damage induced in concrete and infill materials at the peak flexural loads of the modelled columns. All columns exhibited full tensile damage of concrete in the vicinity of midspan region when the peak flexural loads are achieved. However, the distribution of tensile damage in columns CC (FEM-1) and CC-E was dominant compared to other models and this is due to the high confinement efficiency provided by the GFRP wrap which allowed for utilizing the concrete damage to be distributed all through the bottom side of columns upon attaining the peak. Nevertheless, columns CC (FEM-2) and CC-CM as well as column UC showed a low dominant effect with respect to the tensile damage of concrete which is substantially concentrated in the midspan region. Fig. 17b shows the compressive damage in infills at peak flexural loads whereas a remarkable distribution of compressive stresses is observed in column CC-CM compared to that of column CC-E and this indicates the low confinement effect of GFRP wrap in column CC-CM.

Fig. 18 shows the damage criterions of GFRP in the longitudinal and circumferential directions of the modelled columns. The damage is visualized in terms of the maximum value of the fibre “HSNFTCRT” and matrix “HSNMTCRT” tensile initiation criterions which were achieved during the FEM analysis [69]. These damage criterions can have a value ranges from 0 when there is no damage of composite up to a maximum value of 1 when full damage occurs. The damage of GFRP composite in the longitudinal direction of column CC (FEM-1) was the highest among the other models indicating the effective stress transfer from concrete substrate to the surrounding GFRP wrapping. In contrary, the FEM model of column CC (FEM-2) showed a reduction of yield load by 21% compared to column CC (FEM-1) with a considerable increase by 157% and a reduction by 71% in the strain of tensile and compressive steel bars, respectively as detailed in Table 9. This performance reveals that the loss of bond with the GFRP wrap could result in a significant influence on the flexural performance of wrapped columns. Moreover, a related performance can be also noted in column CC-CM, whereas the highest tensile strain at peak was reported to be 40,565 microstrains.

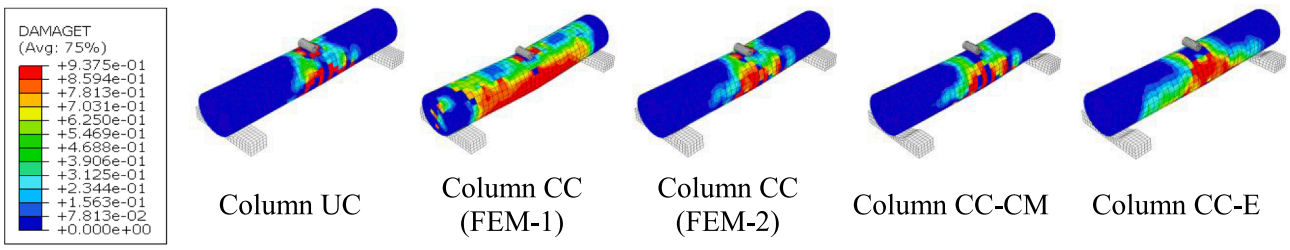

Fig. 16. Tensile damage in concrete at peak flexural loads.

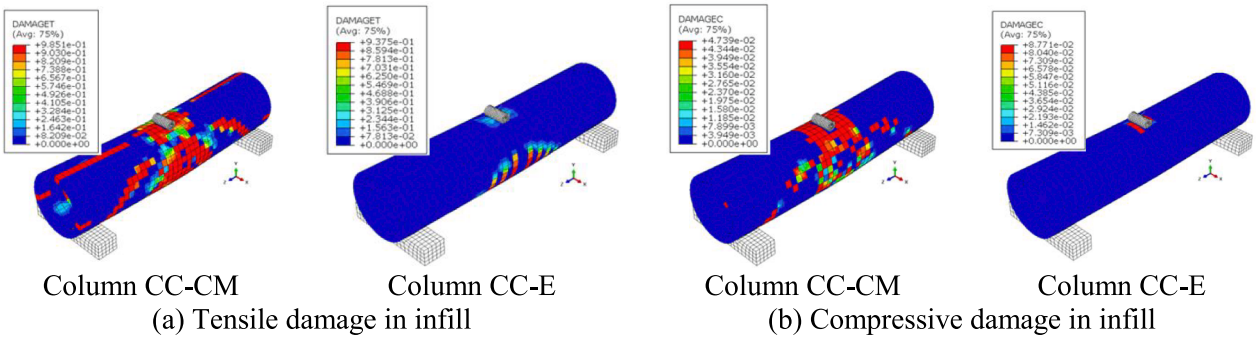

Fig. 17. Tensile and compressive damage in infills at peak flexural loads.

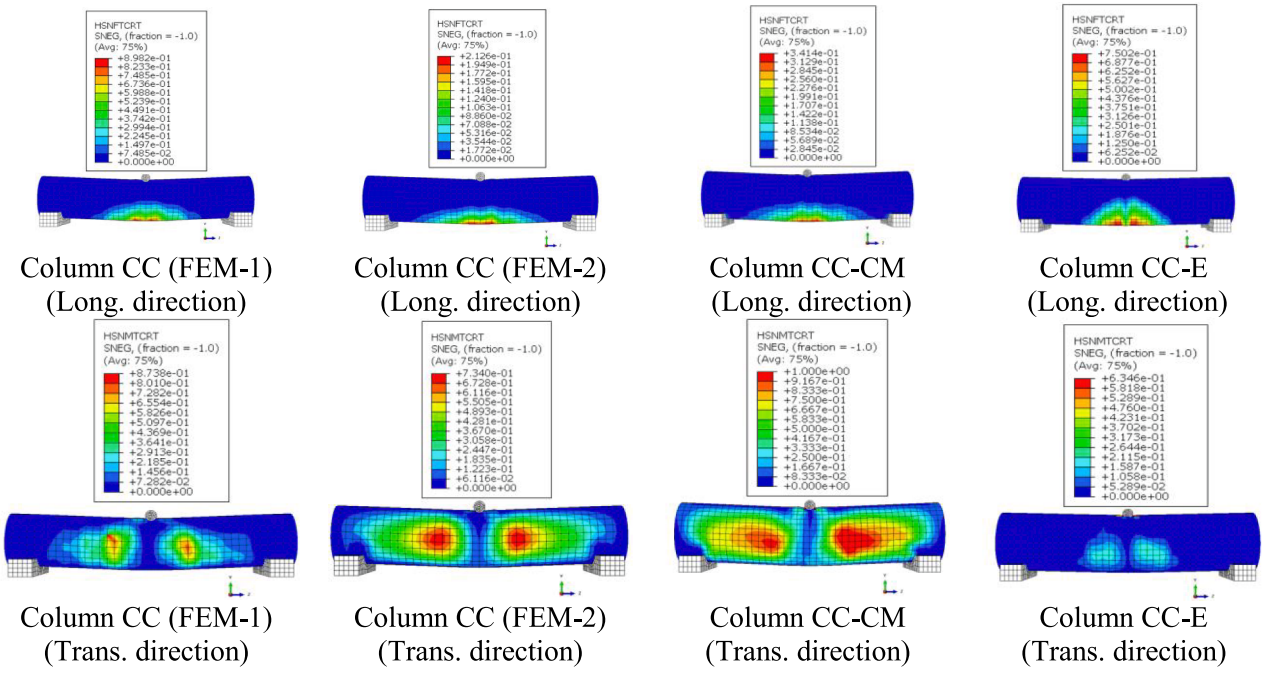

Fig. 18. GFRP tension failure in longitudinal and transverse directions at peak flexural loads.

These high strain values could be attributed to the weak bond with the surrounding GFRP wrap, which effectively results in decreasing the tensile damage of GFRP composite in longitudinal direction as shown in Fig. 18, and consistently increasing this damage in the transverse (circumferential) direction for columns CC (FEM-2) and CC-CM. Therefore, this performance would cause the stress transfer to be excessively directed to the bottom longitudinal bars and thus, increase the induced strains. In contrast, this behaviour is not dominant in columns CC (FEM-1) and CC-E whereas more consistent distribution is observed in the composite damage in both directions.

Despite that longitudinal tensile reinforcement of column CC-E yielded at a flexural load much higher than that for column CC-CM, the post yield performance of CC-E presented a stiffer response to reach a strain of 11,743 microstrains at the peak flexural load, which is significantly lower than that for column CC-CM. Furthermore, a similar response is also revealed in the strains of the compressive longitudinal reinforcement with a reduction of 62% reported for column CC-E compared to column CC-CM as presented in Table 9. Possible reason for this response is that the low tensile strength of grout infill would result in early tensile crushing of grout material, which could eventually increase the stresses sustained by steel bars and thus inducing high tensile and compressive strains. This can be noted in the wide distribution of tensile damage in grout infill in contrast to that of epoxy infill (Fig. 17a). Above all, compressive reinforcement exhibited strains lower than yield strain in GFRP-wrapped columns with infills as shown in Fig. 15, however, higher compressive strains were reported for column CC-CM. This is attributed to the enlargement of the cross section due to the use of infill which provided a larger compression area and thus obtaining a higher capability to sustain the applied stresses in the compression zone. This behaviour evinces that providing an infill material in the GFRP wrapping system is sufficient in confining concrete in the compression zone from expansion that might develop due to widening of cracks.

5. Theoretical analysis

5.1. Development of model

A simplified theoretical analysis was developed using the conventional beam theory to evaluate the flexural capacities of the tested columns. The developed analysis was based on the following assumptions, (1) sections normal to neutral axis remain plane after bending, (2) concrete and infill materials under tension were assumed not to have a contribution to the section capacity, (3) the steel bars are effective in carrying tensile and compressive forces, (4) failure of columns is consequent with the compression crushing of either concrete or infill, i.

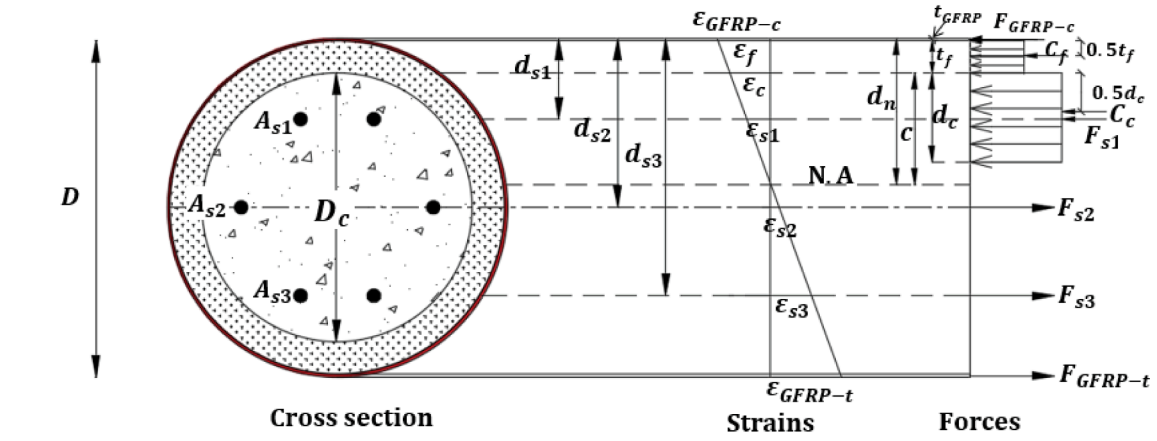

(a) Details of strains and forces of column cross section

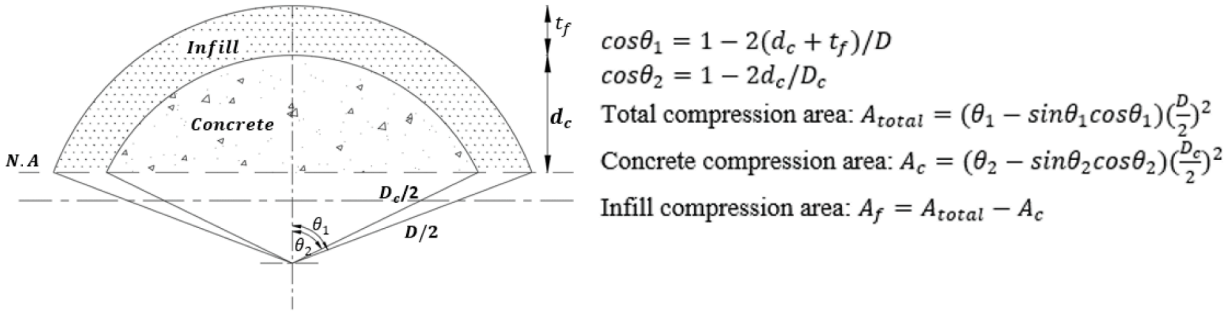

(b) Area of compression segments

Fig. 19. Theoretical analysis.

e. the material of lower peak compressive strain and (5) strain compatibility in the cross section with perfect bond assumed between the different materials. The properties of constitutive materials listed in Table 4 were incorporated in this analysis. Fig. 19a presents the details of the cross section of the circular GFRP-wrapped columns, strains, and forces, where the neutral axis (N.A) is located at depth (d_n) from the most top fibre of the section.

The analysis starts by establishing the lowest compressive strain at peak in either concrete or infill. This implies that concrete crushing was supposed to occur in columns UC, CC, and CC-E but grout crushing to be the failure of column CC-CM. After that, the strains in the constitutive materials can be computed using the linear strain distribution assumed through the section, such that to get equilibrium of forces acting on the section i.e., the tensile forces equal to the compressive forces. This requires an iterative procedure by assuming the depth of neutral axis and calculating the corresponding strains so, an MS excel sheet was developed for this purpose and to calculate the applied forces and moment capacity of the sections.

For columns with the assumption of failure by concrete crushing, the internal compressive force in concrete block (C_c) at the top of the section was based on the equivalent stress distribution which approximates the nonlinear stress block by an equivalent rectangular compressive stress block to simplify the analysis calculations and can be obtained by Eq. (12).

$$C_c = \alpha f_c^{'} A_c \tag{12}$$

where α is the fraction of uniform stress to the peak stress of concrete and given by $\alpha = 1.0 - 0.003 f_c^{'}$ such that $0.67 \le \alpha \le 0.85$, $f_c^{'}$ is the compressive strength of concrete, A_c is the area of the concrete segment and computed as shown in Fig. 19b where $D = D_c + 2t_f$ is the inner diameter of wrapped columns and D_c is the diameter of concrete column. The depth of the assumed rectangular compressive stress block (d_c) is a fraction of the depth of the neutral axis i.e., $d_c = \gamma c$, where γ is given by $\gamma = 1.05 - 0.007 f_c^{'}$ such that $0.67 \le \gamma \le 0.85$ and c is the depth of the topmost compression fibre of concrete to the neutral axis and given by $c = d_n - t_f - t_{GFRP}$, where t_f and t_{GFRP} are the thickness of infill and GFRP, respectively. The factors α and γ are based on AS3600-2009 Standards [52]. The internal compressive force in the infill segment (C_f) at the top of the section was obtained by using the expressions given in Eq. (13).

$$C_f = f_f A_f \tag{13a}$$

$$f_f = E_f(\varepsilon_f + \varepsilon_{cu})/2 \tag{13b}$$

$$\varepsilon_f = \frac{\varepsilon_{cu}}{c}(d_n - t_{GFRP}) \tag{13c}$$

where f_f is the infill compressive stress, E_f and ε_f are the modulus of elasticity and strain in the topmost fibre of infill, respectively,ε_{cu} is the concrete compressive strain at peak and A_f is the area of the infill compression segment in the top side of the section and determined as shown in Fig. 19b. The strain in each steel layer (ε_{si}) can be computed as Eq. (14).

$$\varepsilon_{si} = \frac{\varepsilon_{cu}}{c}(d_{si} - d_n) \tag{14}$$

where d_{si} is the depth from the topmost compression fibre to the centroid of the corresponding steel layer. The positive or negative strains indicate that the steel layer is under tension or compression, respectively. Also, the strain in the top compressive (ε_{GFRP-c}) and bottom tensile (ε_{GFRP-t}) strains in the GFRP jacket can be computed as Eqs. (15) and (16), respectively.

$$\varepsilon_{GFRP-c} = \frac{\varepsilon_{cu}}{c} d_n \tag{15}$$

$$\varepsilon_{GFRP-t} = \frac{\varepsilon_{cu}}{c}(D + 2t_{GFRP} - d_n) \tag{16}$$

After determining the strains, the internal forces can be obtained as follows. The tensile forces in steel bars F_{si} were computed as Eq. (17).

$$F_{si} = A_{si} f_{si} \tag{17}$$

where $f_{si} = E_s \varepsilon_{si} \leq f_y$ is the tensile stress in steel bars, A_{si} is the area of the two steel bars in each layer,E_s and f_y are the modulus of elasticity and yield strength of steel, respectively. In addition, the internal forces in the top and bottom GFRP (F_{GFRP}) are determined as Eq. (18).

$$F_{GFRP} = A_{GFRP} f_{GFRP} \tag{18}$$

where$f_{GFRP} = E_{GFRP}\varepsilon_{GFRP} \leq f'_{GFRP}$is the tensile or compressive stress in GFRP, A_{GFRP} is the area of GFRP and calculated as the multiplication of the thickness of the jacket with the perimeter length of the tension sector to get F_{GFRP-t} or the compression sector to get F_{GFRP-c}, E_{GFRP} and f'_{GFRP} are the modulus of elasticity and the tensile strength of GFRP in the longitudinal direction of column and set to be as the values listed in Table 6 and Table 7.

Likewise, for columns with the assumption of failure by infill crushing, the internal compressive force in infill block (C_f) at the top of the section was obtained by Eq. (19).

$$C_f = f'_f A_f \tag{19}$$

where f'_f is the compressive strength of infill. The internal compressive force in the concrete (C_c) at the top of the section can be obtained by Eq. (20).

$$C_c = \alpha f'_c A_c \tag{20}$$

where f_c is the concrete compressive stress and computed as Eq. (21) [71].

$$f_c = f'_{co}\left[\frac{2\varepsilon_c}{\varepsilon_{cu}} - \left(\frac{\varepsilon_c}{\varepsilon_{cu}}\right)^2\right] \tag{21}$$

where f'_{co} is the compressive strength of concrete and ε_c is the strain in the top fibre of concrete and calculated as Eq. (22).

$$\varepsilon_c = \frac{\varepsilon_{fu}}{d_n - t_{GFRP}} c \tag{22}$$

where ε_{fu} is the infill compressive strain at peak. Similarly, the strains in steel bars, top and bottom GFRP can be calculated as Eqs. (23), (24) and (25), respectively. Also, the forces in steel bars, top and bottom GFRP can be computed as previously explained in Eqs. (17) and (18).

$$\varepsilon_{si} = \frac{\varepsilon_{fu}}{d_n - t_{GFRP}}(d_{si} - d_n) \tag{23}$$

$$\varepsilon_{GFRP-c} = \frac{\varepsilon_{fu}}{d_n - t_{GFRP}} d_n \tag{24}$$

$$\varepsilon_{GFRP-t} = \frac{\varepsilon_{fu}}{d_n - t_{GFRP}}(D + 2t_{GFRP} - d_n) \tag{25}$$

Moreover, the confinement contribution to the compressive strength of wrapped concrete and infill was considered in this analysis of columns CC, CC-CM and CC-E and can be represented by one of the available confinement models in literature, however in this study the model proposed by Lam and Teng [80] shown in Eq. (26) was used.

$$\frac{f'_{cc}}{f'_o} = 1 + 2\frac{f_l}{f'_o} \tag{26}$$

$$f_l = \frac{2E_{GFRP,l} t_{GFRP} \varepsilon_{GFRP,l}}{D} \tag{27}$$

where f'_{cc} is the compressive strength of the wrapped concrete or infill,f'_o is the the unwrapped compressive strength i.e. f'_c for concrete and f'_f for infill, f_l is the lateral confining pressure induced by the GFRP wrap and can be computed as Eq. (27), where $E_{GFRP,l}$ is the modulus of elasticity of the GFRP wrap in the circumferential direction of wrapped columns and $\varepsilon_{GFRP,l}$ is the rupture strain of GFRP wrap in the circumferential direction of columns and assumed to be 0.0189 mm/mm as provided by Kaya et al. [14]. The enhancement of wrapping to the compressive strain at peak was also incorporated using the model proposed by Richart et al. [81] shown in Eq. (28), as it is the most commonly used expression [82].

$$\varepsilon_{cc} = 5\varepsilon_o\left(\frac{f'_{cc}}{f'_o} - 0.8\right) \tag{28}$$

where ε_{cc} is the compressive strain corresponded to the peak stress f'_{cc} and ε_o is the compressive strain at stress f'_o. Finally, after achieving the equilibrium of tensile and compressive forces, the moment capacity of the section was determined by taking the moment of forces about the neutral axis according to Eq. (29) and the peak flexural load of columns under the three-point bending was obtained according to Eq. (30).

$$M_{N.A} = \sum_{i=1}^{3} F_{si}|(d_{si} - d_n)| + C_c(c - d_c/2) + C_f\left(c + t_f/2\right) + F_{GFRP-t}(D + 2t_{GFRP} - d_n) + F_{GFRP-c}(d_n) \tag{29}$$

$$P_{peak} = \frac{4M_{N.A}}{L} \tag{30}$$

where L is the clear span of columns. It is worth noting that the flexural capacity values derived from this model are nominal and do not take reduction factors into consideration. Several studies have investigated the significance of using reduction factors [83,84] due to their importance in determining the design capacity of structures. As a result, to produce a safe design, appropriate strength reduction factors must be utilised in accordance with the relevant design standards and codes.

5.2. Theoretical results and comparisons with experimental and FEM work

Table 10 shows a comparison among the peak flexural loads obtained from the theoretical analysis and the results of experimental and FEM analyses. It is evident that there is a good correlation between the results of the column UC which indicates that the assumptions made for this analysis were accurate. However, for the wrapped columns, a good correlation is observable in the peak flexural load between the theoretical and experimental results of columns CC1 and CC-E and this is due to that these columns may perform a good contact between concrete and surrounding wrapping system, which corresponds with the assumptions made in the theoretical analysis. On the other hand, the lack of correspondence in results between the theoretical and experimental results is observed in columns CC2 and CC-CM with an average discrepancy of

Table 10
Comparison of peak flexural loads between theoretical, experimental, and FEM results.

Column	Theoretical	Experimental	FEM		$\frac{P_{Theo}}{P_{EXP}}$	$\frac{P_{Theo}}{P_{FEM-1}}$	$\frac{P_{Theo}}{P_{FEM-2}}$
	P_{Theo}(kN)	P_{EXP} (kN)	P_{FEM-1}(kN)	P_{FEM-2} (kN)			
UC1	127	133	134		0.95	0.94	
UC2		137			0.92		
CC1	306	328	319	232	0.93	0.96	1.32
CC2		214			1.43		
CC-CM1	491	406	479	369	1.21	1.03	1.33
CC-CM2		369			1.33		
CC-E1	512	482	494	364	1.06	1.04	1.41
CC-E2		462			1.11		

32% and this could be traced back to that the strain compatibility and perfect bond assumed in this analysis might not reflect the real behaviour of such columns.

Nevertheless, the comparison between the theoretical results and FEM results which assumed a perfect contact (FEM-1) between infill, concrete, and surrounding wrap showed only a maximum of 4% difference and this indicates the excellent agreement between the theoretical and FEM results in case of perfect bond assumption, anyhow, high discrepancy is observed between the theoretical results and the FEM-2 results. In the analysis discussed in section 4.4.1, the difference with experimental results of columns CC-CM was minor when using the second approach (FEM-2) and was shown to be more accurate in describing the behaviour of indicated columns. However, the first approach (FEM-1) which considers perfect bond exhibited a discrepancy in results (see Fig. 14). Similarly, the experimental results of columns CC-E, which showed no evidence of GFRP separation, corresponded to the model that assumes perfect bonding (FEM-1). Furthermore, the experimental result of column CC2, which showed GFRP separation, matched the model CC-FEM2, which assumes imperfect bonding. While the experimental result of column CC1, which showed no GFRP separation, correlated well with the model CC-FEM1, which assumes perfect bonding. As a result, the theoretical analysis which only considers perfect bonding between the different materials, cannot predict such behaviour; therefore, including the FEM analysis is beneficial in predicting the various behaviour of columns and may outperform theoretical analysis in this regard. Further investigations, however, are needed to theoretically study and analyze the influence of the loss of bond between the constituent materials on the overall flexural capacity of the GFRP-wrapped columns.

6. Parametric study and verification of the theoretical model

A parametric analysis was performed to explore the flexural behaviour of columns due to the variation of thickness of the GFRP and infill, as well as changing the loading mode from three-point bending to four-point bending. Since the theoretical model assumes perfect bonding mechanism between constituent materials, the models of GFRP-wrapped columns were developed utilizing the FEM-1 approach described in section 4.3.2.

6.1. Influence of GFRP thickness

Fig. 20 presents the influence of increasing the GFRP thickness from two to four and six layers on the behaviour of columns CC, CC-CM and

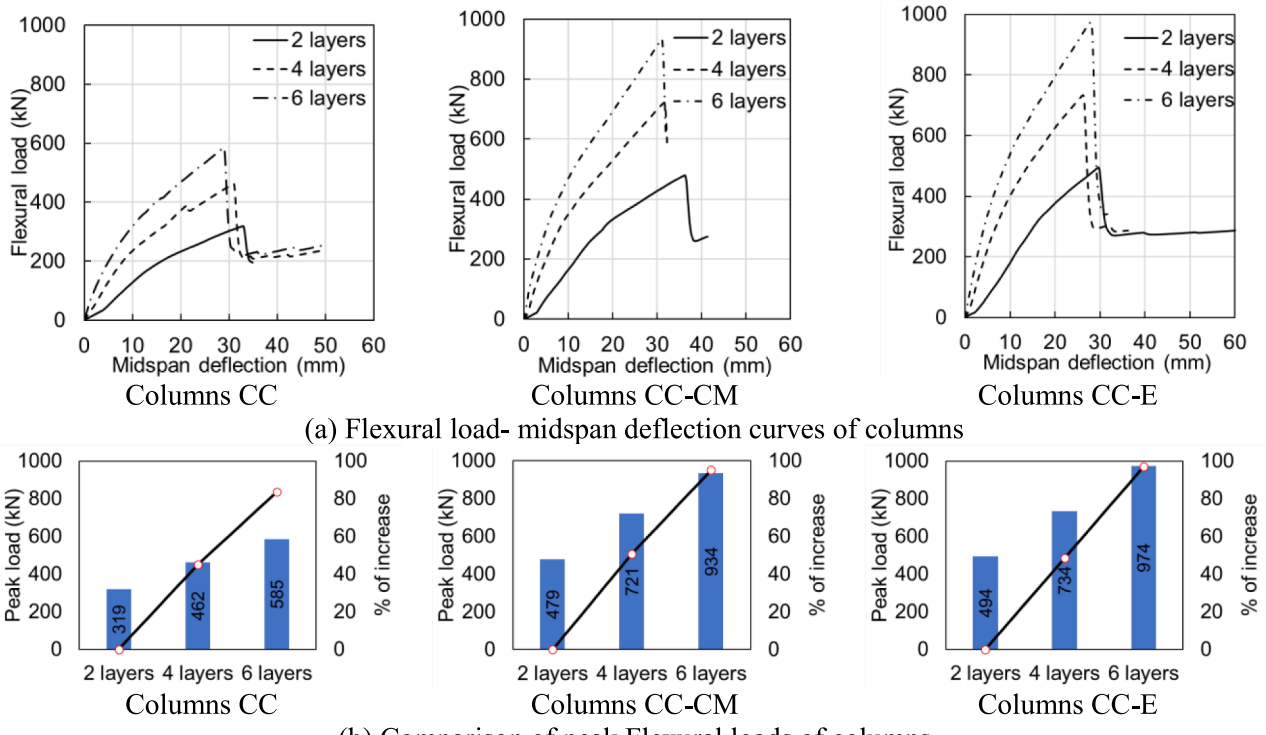

Fig. 20. Influence of GFRP thickness.

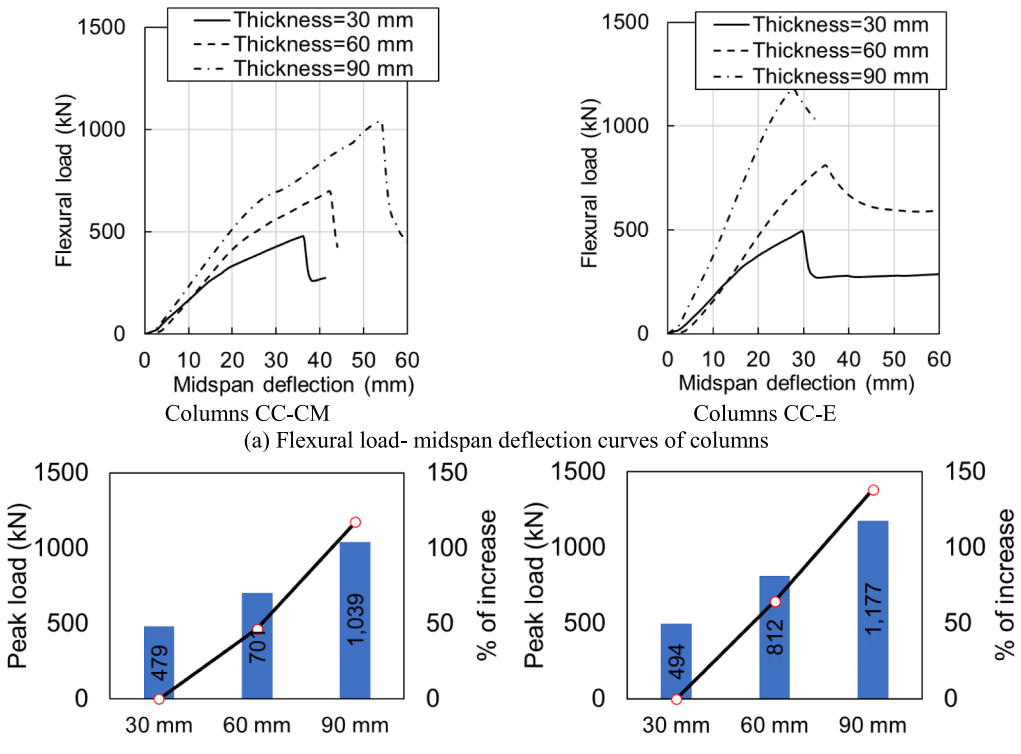

(a) Flexural load- midspan deflection curves of columns

(b) Comparison of peak flexural loads of columns

Fig. 21. Influence of infill thickness.

CC-E. As presented in Fig. 20a, it is observed that the peak flexural loads were significantly improved with the increased number of GFRP layers, while midspan deflections were slightly reduced. Furthermore, as the GFRP thickness is increased, the initial stiffness increases dramatically, demonstrating the effective contribution of GFRP wrapping. Despite that the increases in peak flexural loads with the variation of GFRP thickness are proximate for the various columns, column CC-E with 6 layers exhibits the maximum increase of 97% compared to that with 2 layers (Fig. 20b). This increased strength and stiffness of columns can be due to the confinement effect provided by GFRP layers to the concrete core.

6.2. *Influence of infill thickness*

Fig. 21a shows the flexural load versus midspan deflection curves to illustrate the effect of infill thickness on the flexural behaviour of the GFRP-wrapped columns CC-CM and CC-E with two thicknesses (60 and 90 mm) being investigated. According to the FEM results, the use of a 60 mm thick infill increases the peak flexural load by 46% and 65% for columns CC-CM and CC-E, respectively, while the 90 mm thick infill increases the peak load by 117% and 138% for columns CC-CM and CC-E, respectively as presented in Fig. 21b. In comparison to columns CC-E, the large rise in midspan deflection with increasing infill thickness for columns CC-CM demonstrates the higher ductility performance of these columns. Furthermore, due to the high rigidity of epoxy infills, increasing the infill thickness in columns CC-E to 90 mm significantly increases the stiffness of GFRP wrapped columns. The increase in stiffness and strength with the increase in infill thickness can be due to the increased moment of inertia of the column section and the increased stiffness provided by the GFRP wrapping.

6.3. *Influence of variation of loading from three-point to four-point bending*

A numerical comparison was conducted to explore the difference in behaviour of columns under the effect of two loading modes. The numerical models were modified so that the columns are subjected to a four-point bending with a shear span of $L/3$. The flexural load versus midspan deflection curves of columns UC, CC, CC-CM and CC-E are presented in Fig. 22a. As to be expected, columns under four-point bending could sustain higher flexural loads due to the reduction of the shear span length. The change of loading mode to four-point bending results in increasing the peak flexural loads by a percentage ranging between 41% and 57% for columns CC-CM and UC, respectively, as indicated in Fig. 22b. It is evident that the four-point bending could substantially increase the slope of flexural load midspan deflection of all columns compared to that of three-point bending, indicating their stronger resistance for deflection under the applied loads. This can be demonstrated using the general Eq. (31).

$$\frac{P}{\delta} = \frac{48EI}{a(3L^2 - 4a^2)} \tag{31}$$

where a is the shear span length which is the distance between the support and point load, L is the span length, P is the applied load, δ is the corresponding deflection and EI is the flexural stiffness which is a function of modulus of elasticity and moment of inertia of the section. Since the columns are similar in terms of geometry and cross-sectional properties under the two loading modes, the smaller the shear span length, the larger the load required to achieve the same deflection. As a result, columns subjected to four-point bending exhibit smaller deflections under the same applied load compared to those subjected to three-point bending. Additionally, it is noted that the reduction in shear span in columns subjected to four-point bending delays the failure development within the region of maximum moment due to the stabilised stress distribution compared to those subjected to three-point bending. This may be determined by looking at GFRP failure in the longitudinal direction of columns (Fig. 22c), where the results show that the GFRP has full damage (HSNFTCRT = 1.00) when the peak load is achieved, which is evidently higher than what was indicated in columns under three-point bending previously illustrated in Fig. 18.

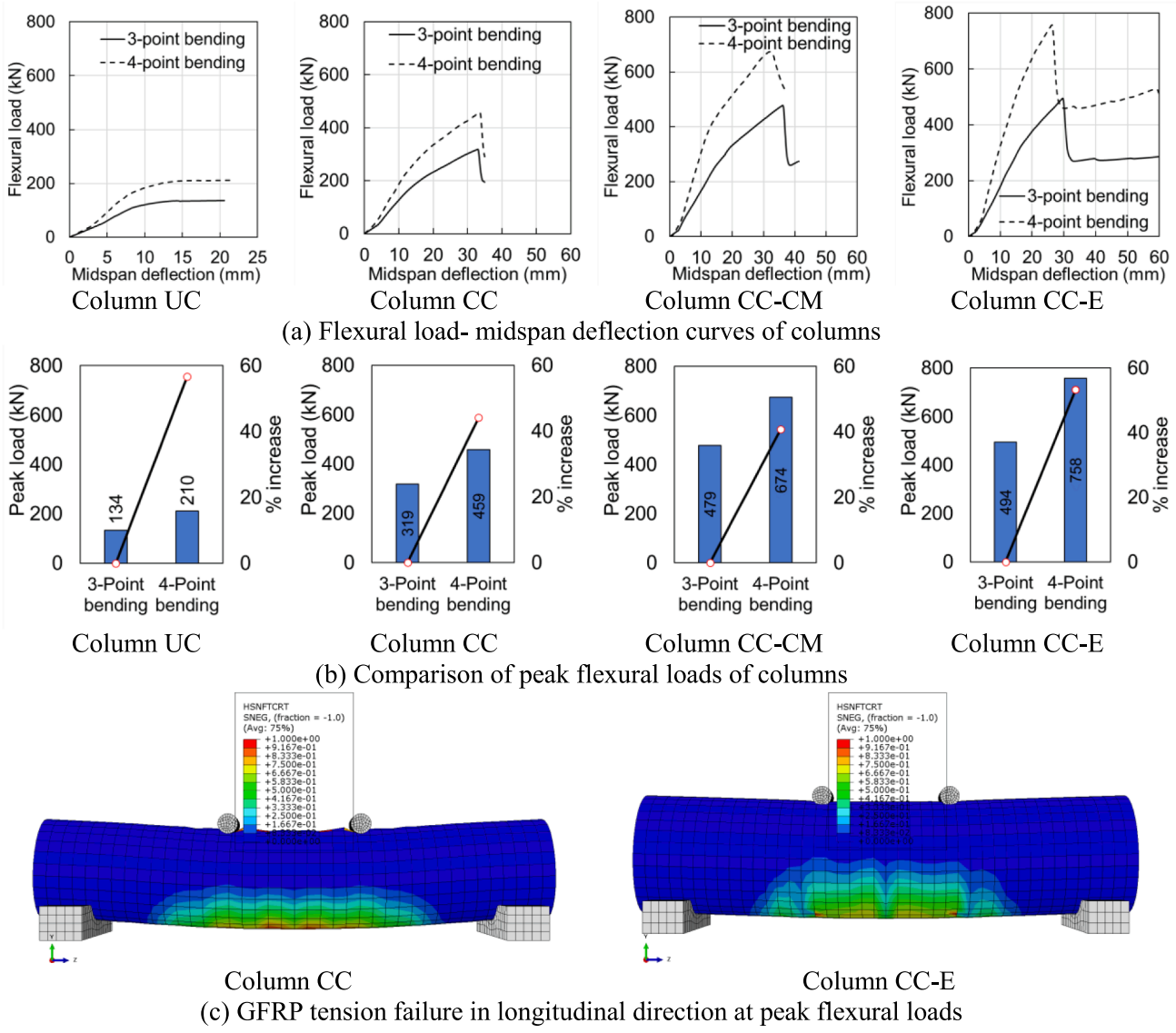

Fig. 22. Influence of variation the loading from three-point to four-point bending.

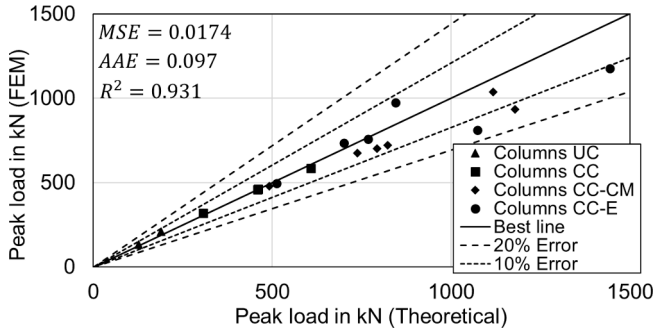

Fig. 23. Comparison between FEM and theoretical results for the peak flexural loads.

Furthermore, the results for column CC-E reveal that there was no compressive damage in the infill at peak load; nevertheless, this damage began to develop at 95% of the peak load in the post peak region. On the other hand, the results of the three-point bending showed that epoxy infill started to experience compressive damage before the peak load. As a result, columns under four-point bending may exhibit more stable stress distribution and failure within the constituent materials, but three-point bending provides the optimum condition for the column performance since the concentrated load at midspan induces the worst bending conditions.

6.4. Verification of developed theoretical model with the results of parametric study

Fig. 23 shows a comparison between the peak load of columns as determined by parametric analysis and their estimated values as determined by the theoretical model developed in section 5.

Three statistical indicators were employed to assess the performance of the models: the mean square error (MSE), the average absolute error (AAE) and the coefficient of determination (R^2), defined in Eqs. (32), (33) and (34), respectively. Low MSE and AAE values imply higher model performance, while an R^2 value of one indicates the best

correlation.

$$MSE = \frac{\sum_{i=1}^{N}\left(\frac{x-y}{y}\right)^2}{N} \quad (32)$$

$$AAE = \frac{\sum_{i=1}^{N}\left|\left(\frac{x-y}{y}\right)\right|}{N} \quad (33)$$

$$R^2 = \left[\frac{n\sum xy - \sum x\sum y}{\sqrt{(n\sum x^2 - (\sum x)^2)(n\sum y^2 - (\sum y)^2)}}\right]^2 \quad (34)$$

where $\times$ and y represent the theoretical and FEM values of peak loads, respectively. As evidenced by the findings, the high precision values of MSE, AAE, and R^2 show that the developed theoretical model performs reasonably well in estimating the peak flexural loads of the various modelled columns. As a result, the model's accomplishment demonstrates its precision and applicability in predicting the performance of columns which exhibit perfect bond between the constituent materials.

7. Conclusion

The behaviour of GFRP-wrapped RC columns was studied under the effect of three-point static bending in this study. Experimental works were carried out accompanied with FEM simulation and theoretical prediction. Based on the results of experiments, FEM and theoretical analyses, the following conclusions can be drawn:

1. The tensile fracture of the composite jacket in the longitudinal direction governs the failure of GFRP-wrapped columns under bending. The GFRP wrapping system provided significant external reinforcement to RC columns, improving their flexural performance by up to 250%.
2. The flexural behaviour of GFRP-wrapped columns is considerably affected by the properties of the infill material. Columns with epoxy infills have the highest peak strengthening while columns with grout infills have the highest ductility and energy absorption.
3. The developed 3D finite element models which consider the nonlinear behaviour of concrete, grout and epoxy materials can adequately predict the load-deflection response of the GFRP-wrapped columns under bending. The FEM predicted failure modes are in good correlation with those observed in experiments.
4. The results of the numerical model, which considers a non-perfect bond between grout infill and both concrete and surrounding GFRP wrap, match reasonably with the experimental results. This reiterates the importance of having good bonding between grout infill and concrete as well as the same with GFRP wrap.
5. The results of the theoretical analysis developed using the conventional beam theory have a discrepancy in wrapped columns with grout infills when compared to experimental results, implying that the strain compatibility used in the analysis may not accurately reflect the real behaviour of such columns.
6. The parametric study indicates that increasing the number of GFRP layers remarkably enhances the stiffness of columns, whilst increasing the thickness of infill significantly increases the flexural capacity of columns. The results also reveal that using four-point bending can delay the failure of constituent materials due to improved stress dispersion within the column.

The above findings suggest the effectiveness of GFRP wrapping systems in enhancing the flexural performance of RC columns. Proposed theoretical analysis, validated by experimental and FEM analysis could be useful for practising engineers in designing FRP strengthening systems for column. Further development is, however, recommended to achieve sufficient bond between grout infills and both the substrate concrete columns and GFRP wrap.

Research data

The raw/processed data required to reproduce these findings cannot be shared at this time as the data also forms part of an ongoing study.

Declaration of Competing Interest

The authors declare that they have no known competing financial interests or personal relationships that could have appeared to influence the work reported in this paper.

Acknowledgments

The authors are grateful to Innovation Connections (IC) by the Australian Government for their financial support of this study (Grant No. ICG000869). The first author acknowledges the support received through the research training program (RTP) Stipend scholarship. The authors would like to acknowledge the support of QuakeWrap Pty. Ltd., Australia for the materials supply, casting of samples and providing technical support. Also, sincere thanks for the technical staff at the Centre for Future Material (CFM), University of Southern Queensland, Toowoomba for their assistance in conducting the experimental work of this study.

References

[1] Garzón-Roca J, Adam JM, Calderón PA. Behaviour of RC columns strengthened by steel caging under combined bending and axial loads. Constr Build Mater 2011;25(5):2402–12.
[2] Ghernouti Y, Li A, Rabehi B. Effectiveness of repair on damaged concrete columns by using fiber-reinforced polymer composite and increasing concrete section. J Reinf Plast Compos 2012;31(23):1616–29.
[3] Wu Y-F, Liu T, Oehlers DJ. Fundamental Principles that Govern Retrofitting of reinforced concrete columns by steel and FRP jacketing. Adv Struct Eng 2006;9(4):507–33.
[4] Karbhari VM, Gao Y. Composite jacketed concrete under uniaxial compression-verification of simple design equations. J. Mater. Civ. Eng. 1997;9(4):185–93.
[5] Purushotham Reddy B, Alagusundaramoorthy P, Sundaravadivelu R. Retrofitting of RC piles using GFRP composites. KSCE J Civ Eng 2009;13(1):39–47.
[6] QuakeWrap Inc., https://quakewrap.com.au/pilemedic/.
[7] Liu X, Nanni A, Silva PF. Rehabilitation of compression steel members using FRP pipes filled with non-expansive and expansive light-weight concrete. Adv Struct Eng 2005;8(2):129–42.
[8] Berthet JF, Ferrier E, Hamelin P. Compressive behavior of concrete externally confined by composite jackets. Part A: experimental study, Construction and Building Materials 2005;19(3):223–32.
[9] Lam L, Teng JG. Design-oriented stress–strain model for FRP-confined concrete. Constr Build Mater 2003;17(6-7):471–89.
[10] Rochette P, Labossière P. Axial Testing of Rectangular Column Models Confined with Composites. J Compos Constr 2000;4(3):129–36.
[11] Mohammed AA, Manalo AC, Maranan GB, Zhuge Y, Vijay PV. Comparative study on the behaviour of different infill materials for pre-fabricated fibre composite repair systems. Constr Build Mater 2018;172:770–80.
[12] Hadi MNS, Algburi AHM, Sheikh MN, Carrigan AT. Axial and flexural behaviour of circular reinforced concrete columns strengthened with reactive powder concrete jacket and fibre reinforced polymer wrapping. Constr Build Mater 2018;172:717–27.
[13] Vijay PV, Soti PR, GangaRao HVS, Lampo RG, Clarkson JD. Repair and Strengthening of Submerged Steel Piles Using GFRP Composites. J Bridge Eng 2016;21(7):04016038. https://doi.org/10.1061/(ASCE)BE.1943-5592.0000903.
[14] Kaya A, Dawood M, Gencturk B. Repair of corroded and buckled short steel columns using concrete-filled GFRP jackets. Constr Build Mater 2015;94:20–7.
[15] Beddiar A, Zitoune R, Collombet F, Grunevald YH, Abadlia MT, Bourahla N. Compressive behaviour of concrete elements confined with GFRP-prefabricated bonded shells. European Journal of Environmental and Civil Engineering 2015;19(1):65–80.
[16] Hadi MNS, Khan QS, Sheikh MN. Axial and flexural behavior of unreinforced and FRP bar reinforced circular concrete filled FRP tube columns. Constr Build Mater 2016;122:43–53.
[17] Lokuge W, Otoom O, Borzou R, Navaratnam S, Herath N, Thambiratnam D. Experimental and numerical analysis on the effectiveness of GFRP wrapping system on timber pile rehabilitation. Case Stud Constr Mater 2021;15:e00552. https://doi.org/10.1016/j.cscm.2021.e00552.
[18] Mohammed AA, Manalo AC, Maranan GB, Zhuge Y, Vijay PV, Pettigrew J. Behavior of Damaged Concrete Columns Repaired with Novel FRP Jacket. J Compos Constr 2019;23(3):04019013. https://doi.org/10.1061/(ASCE)CC.1943-5614.0000942.

[19] Menkulasi F, Baghi H, Hall D, Farzana N. Rehabilitation of deteriorated timber piles using FRP composites. Southern Plains Transportation Center-The University of Oklahoma; 2017.
[20] Karagah H. FRP-Confined Grout Systems for Underwater Rehabilitation of Corroded Steel Bridge Piles, Faculty of the Department of Civil and Environmental Engineering. University of Houston; 2015.
[21] Li G, Kidane S, Pang S-S, Helms JE, Stubblefield MA. Investigation into FRP repaired RC columns. Compos Struct 2003;62(1):83–9.
[22] M. Murugan, K. Muthukkumaran, C. Natarajan, FRP-Strengthened RC Piles. I: Piles under Static Lateral Loads, Journal of Performance of Constructed Facilities 31(3) (2017) 04017003-14.
[23] Lopez-Anido R, Michael AP, Sandford TC. Experimental characterization of FRP composite-wood pile structural response by bending tests. Mar struct 2003;16(4): 257–74.
[24] Do TV, Pham TM, Hao H. Dynamic responses and failure modes of bridge columns under vehicle collision. Eng Struct 2018;156:243–59.
[25] Zhang X, Hao H, Li C. Experimental investigation of the response of precast segmental columns subjected to impact loading. Int J Impact Eng 2016;95:105–24.
[26] Queensland Government Department of Transport and Main Roads, Structure Inspection Manual, Part 2: Deterioration Mechanisms https://www.tmr.qld.gov.au/business-industry/Technical-standardspublications/Structures-Inspection-Manual, 2016.
[27] Anwar N, Fawad Ahmed N. Structural Cross-Sections, Elsevier 2017.
[28] Ahmad J, Ali S, Yu T, Sheikh MN, Hadi MNS. Analytical investigation on the load-moment interaction behavior of the FRP reinforced geopolymer concrete filled FRP tube circular columns, Journal of Building. Engineering 2021;42:102818. https://doi.org/10.1016/j.jobe.2021.102818.
[29] Chellapandian M, Prakash SS. Axial Compression-Flexure Interaction Behavior of Hybrid FRP-Strengthened Columns. ACI Struct J 2019;116(2).
[30] Khorramian K, Sadeghian P. Hybrid system of longitudinal CFRP laminates and GFRP wraps for strengthening of existing circular concrete columns. Eng Struct 2021;235:112028.
[31] Pham TM, Doan LV, Hadi MNS. Strengthening square reinforced concrete columns by circularisation and FRP confinement. Constr Build Mater 2013;49:490–9.
[32] Buth CE, Williams WF, Brackin MS, Lord D, Geedipally SR, Abu-Odeh AY. Analysis of large truck collisions with bridge piers: phase 1, report of guidelines for designing bridge piers and abutments for vehicle collisions. Texas Transportation Institute 2010.
[33] Mohammed AA, Manalo AC, Maranan GB, Muttashar M, Zhuge Y, Vijay P, et al. Effectiveness of a novel composite jacket in repairing damaged reinforced concrete structures subject to flexural loads. Compos Struct 2020;233:111634.
[34] M.R. Ehsani, Repair and strengthening of piles and pipes with FRP laminates, United States Patents No: US 9,376,782 B1, 2016.
[35] Ehsani Mo. FRP super laminates present unparalleled solutions to old problems. Reinf Plast 2009;53(6):40–5.
[36] Saadatmanesh H, Ehsani MR, Jin L. Repair of Earthquake-Damaged RC Columns withFRP Wraps. ACI Struct J 1997;94(2):206–14.
[37] QuakeWrap Inc., http://www.quakewrap.com/index.php.
[38] Otoom OF, Lokuge W, Karunasena W, Manalo AC, Ozbakkaloglu T, Thambiratnam D. Experimental and numerical evaluation of the compression behaviour of GFRP wrapped infill materials. Case Stud Constr Mater 2021;15: e00654. https://doi.org/10.1016/j.cscm.2021.e00654.
[39] Berthet JF, Ferrier E, Hamelin P. Compressive behavior of concrete externally confined by composite jackets: Part B: modeling. Constr Build Mater 2006;20(5): 338–47.
[40] Mohamed HM, Masmoudi R. Flexural strength and behavior of steel and FRP-reinforced concrete-filled FRP tube beams. Eng Struct 2010;32(11):3789–800.
[41] Yan Z, Pantelides CP. Fiber-reinforced polymer jacketed and shape-modified compression members: II-model. ACI Struct J 2006;103(6):894–903.
[42] Mohammed AA, Manalo A, Ferdous W, Abousnina R, AlAjarmeh O, Vijay PV, et al. Design considerations for prefabricated composite jackets for structural repair: Parametric investigation and case study. Composite Structures (30) 2021;261: 113288. https://doi.org/10.1016/j.compstruct.2020.113288.
[43] Youssef MN, Feng MQ, Mosallam AS. Stress–strain model for concrete confined by FRP composites. Compos B Eng 2007;38(5):614–28.
[44] Mohamed HM, Masmoudi R. Axial load capacity of concrete-filled FRP tube columns: Experimental versus theoretical predictions. J Compos Constr 2010;14 (2):231–43.
[45] Yu T, Teng JG, Wong YL, Dong SL. Finite element modeling of confined concrete-II: Plastic-damage model. Eng Struct 2010;32(3):680–91.
[46] Fahmy MF, Wu Z. Evaluating and proposing models of circular concrete columns confined with different FRP composites. Compos B Eng 2010;41(3):199–213.
[47] Roudane B, Kaya A, Adanur S. Numerical investigation of corroded short steel piles repaired using grout-filled FRP jackets, International Civil Engineering and Architectural Conference (ICEARC'19). Turkey 2019:1196–203.
[48] Raza A, Rehman Au, Masood B, Hussain I. Finite element modelling and theoretical predictions of FRP-reinforced concrete columns confined with various FRP-tubes. Structures 2020;26:626–38.
[49] Raza A, Ali B, Nawaz MA, Ahmed I. Structural performance of FRP-RC compression members wrapped with FRP composites. Structures 2020;27:1693–709.
[50] Chen C, Wang X, Sui L, Xing F, Chen X, Zhou Y. Influence of FRP thickness and confining effect on flexural performance of HB-strengthened RC beams. Compos B Eng 2019;161:55–67.
[51] Chellapandian M, Prakash SS, Sharma A. Axial compression–bending interaction behavior of severely damaged RC columns rapid repaired and strengthened using hybrid FRP composites. Constr Build Mater 2019;195:390–404.
[52] AS3600-2009, AS3600-2009, Concrete structures, Australian Standard,Sydney, NSW, 2009.
[53] PileMedic, Technical Data Sheet, PileMedic™ PLG60.60, for Structural Strengthening of Columns and Submerged Piles https://quakewrap.com.au/wp-content/uploads/2015/07/PileMedic-eePLG60.60.pdf.
[54] QuakeBond™ 220UR, Technical Data Sheet, QuakeBond™ 220UR Underwater Resin, https://quakewrap.com.au/wp-content/uploads/2015/07/QuakeBond-220UR-Underwater-Resin.pdf.
[55] ASTM international 2017.
[56] AS1012.9-2014, AS1012.9-2014, Compressive strength tests— Concrete, mortar and grout specimens, Australian Standard,Sydney,NSW, 2014.
[57] Fosroc®Conbextra® UW, Technical Data Sheet, Fosroc® Conbextra® UWGrout, https://www.fosroc.com.au/sites/default/files/2021-01/Fosroc_Conbextra_UW_TDS.pdf, 2020.
[58] QuakeWrap, Technical Data Sheet, QuakeWrap UW Pile Jacket Epoxy Grout (PJE), quakewrap.com.au.
[59] AS/NZS4671, Australian/New Zealand Standard, Steel reinforcing materials, Sydney ,Australia, 2001.
[60] Hawileh RA, Nawaz W, Abdalla JA. Flexural behavior of reinforced concrete beams externally strengthened with Hardwire Steel-Fiber sheets. Constr Build Mater 2018;172:562–73.
[61] Stephen P, Annette P. Axial Load Behavior of LargeScale Spirally Reinforced HighStrength Concrete Columns. ACI Struct J 1997;94(3).
[62] Ahmad J, Yu T, Hadi MN. Behavior of GFRP bar reinforced geopolymer concrete filled GFRP tube columns under different loading conditions. Structures 2021;33: 1633–44.
[63] Al-Nimry H, Neqresh M. Confinement effects of unidirectional CFRP sheets on axial and bending capacities of square RC columns. Eng Struct 2019;196:109329.
[64] Attari N, Amziane S, Chemrouk M. Flexural strengthening of concrete beams using CFRP, GFRP and hybrid FRP sheets. Constr Build Mater 2012;37:746–57.
[65] Fantilli AP, Iori I, Vallini P. Size effect of compressed concrete in four point bending RC beams. Eng Fract Mech 2007;74(1–2):97–108.
[66] Jumaa GB, Yousif AR. Numerical modeling of size effect in shear strength of FRP-reinforced concrete beams. Structures 2019;20:237–54.
[67] Said M, Shanour AS, Mustafa T, Abdel-Kareem AH, Khalil MM. Experimental flexural performance of concrete beams reinforced with an innovative hybrid bars. Eng Struct 2021;226:111348.
[68] Wang F, Wang J, Yang H, Shen Q. Axial compressive behaviour of RC columns strengthened with rectangular steel tube and cementitious grout jackets. Structures 2021;31:484–99.
[69] ABAQUS, ABAQUS, Dassault Systems Simulia, Providence, RI., 2019.
[70] Massicotte B, Elwi AE, MacGregor JG. Tension-stiffening model for planar reinforced concrete members. J Struct Eng 1990;116(11):3039–58.
[71] Warner RF, Rangan BV, Hall AS, Faulkes KA. Concrete Structures. Melbourne: Addison Wesley Longman Australia Ltd.; 1998.
[72] AS 1720.1-2010, AS 1720.1-2010, Timber structures Design methods, Australian Standard., 2010.
[73] Hashin Z. Failure criteria for unidirectional fiber composites. J Appl Mech 1980;47: 329–34.
[74] Wright TJ. Sensitivity of Hashin damage parameters for notched composite panels in tension and out-of-plane bending. Oregon State University; 2012.
[75] A. Raza, Q.u.Z. Khan, A. Ahmad, Numerical Investigation of Load-Carrying Capacity of GFRP-Reinforced Rectangular Concrete Members Using CDP Model in ABAQUS, Advances in Civil Engineering 2019 (2019) 1745341.
[76] Alhawamdeh M, Alajarmeh O, Aravinthan T, Shelley T, Schubel P, Mohammad A, et al. Modelling flexural performance of hollow pultruded FRP profiles. Compos Struct 2021;276:114553.
[77] Cui W, Fernando D, Heitzmann M, Gattas JM. Manufacture and structural performance of modular hybrid FRP-timber thin-walled columns. Compos Struct 2021;260:113506.
[78] Eslami H, Jayasinghe LB, Waldmann D. Nonlinear three-dimensional anisotropic material model for failure analysis of timber. Eng Fail Anal 2021;130:105764.
[79] Lokuge W, Abousnina R, Herath N. Behaviour of geopolymer concrete-filled pultruded GFRP short columns. J Compos Mater 2019;53(18):2555–67.
[80] Lam L, Teng JG. Strength Models for Fiber-Reinforced plastic-confined concrete. ASCE structural Journal 2002;128(5):612–23.
[81] Richart FE, Brandtzæg A, Brown RL. A study of the failure of concrete under combined compressive stresses. College of Engineering: University of Illinois at Urbana Champaign; 1928.
[82] Ozbakkaloglu T, Lim JC, Vincent T. FRP-confined concrete in circular sections: Review and assessment of stress–strain models. Eng Struct 2013;49:1068–88.
[83] Esfahani MR, Kianoush MR, Tajari AR. Flexural behaviour of reinforced concrete beams strengthened by CFRP sheets. Eng Struct 2007;29(10):2428–44.
[84] Khalifa ES, Al-tersawy SH. Experimental and analytical investigation for enhancement of flexural beams using multilayer wraps. Compos B Eng 2013;45(1): 1432–40.